Oxidative Two-State Photoreactivity of a Manganese(IV) Complex using NIR Light

Nathan R. East[1], Robert Naumann[1], Christoph Förster[1], Charusheela Ramanan[2,3], Gregor Diezemann[1] and Katja Heinze[1]*

[1] Department of Chemistry, Johannes Gutenberg University, Duesbergweg 10-14, 55128 Mainz, Germany

[2] Department of Physics and Astronomy, Vrije Universiteit Amsterdam, Amsterdam, Netherlands

[3] Max-Planck-Institute for Polymer Research, Mainz, Germany

Supplementary Information

Table of Contents

1. Methods and Materials

General Procedures. Acetonitrile CH_3CN was distilled under argon atmosphere from CaH_2. Butyronitrile $CH_3CH_2CH_2CN$ was dried according to a previously reported procedure.[1] Nitromethane CH_3NO_2, γ-valerolactone $C_5H_8O_2$ and 1,2-butylene carbonate $C_5H_8O_3$ were dried by storing over 25% v/v pre-activated 3 Å molecular sieves for two days, distillation under reduced pressure at 30°C under argon and by three freeze pump thaw cycles to remove oxygen. The arene substrates (from commercial suppliers Acros, Alfa Aesar, Fischer and Sigma-Aldrich) were distilled prior to use. The complex $[Mn(dgpy)_2][PF_6]_4$ was prepared according to a literature procedure.[2]

UV/Vis/NIR spectra were recorded on a Jasco V770 spectrometer using 1.0 cm cells (Hellma, Suprasil) under inert atmosphere.

NMR spectra were recorded on a Bruker Avance DRX 400 spectrometer. The measurements were performed at 400.31 MHz (^1H), 100.05 MHz ($^{13}C\{^1H\}$), 162.04 MHz ($^{31}P\{^1H\}$) and 376.67 MHz (^{19}F); [CD_3CN (^1H, δ = 1.94)].[3]

ATR-IR spectra were recorded with a Bruker ALPHA II FT-IR spectrometer with a platinum Di-ATR module inside an argon-filled glovebox.

ESI mass spectra were recorded on a Micromass Q-TOF-Ultima spectrometer in CH_3CN.

High performance liquid chromatography was performed on a Jasco 2000 series HPLC containing a UV-2075plus detector and a reprosil 100, C18 5 µm reversed phase column (250 x 4.6 mm). Measurements were carried out at 40°C and pH 7 using a CH_3CN/water gradient eluent and the product retention time was compared with an authentic sample. The yield was determined by comparing peak areas.

Conductivities were measured with a Greisinger conductivity cell, model 6MH 3431 LFE-210 with platinum electrodes in dry acetonitrile under inert atmosphere. The equivalent conductivity Λ_e was plotted as a function of $c^{0.5}$. To determine Λ_0, Λ_e was linearly extrapolated to infinite dilution.

Variable temperature steady-state emission spectra were recorded with a FLS1000 spectrometer from *Edinburgh Instruments* equipped with the cooled, red and NIR sensitive photomultiplier detectors PMT-980 and N-G09 PMT-1700. The CW lasers RLTMDL-730-1W-3 and RLTMDL-635-1W-3 from *Roithner Lasertechnik* were employed for excitation. For the sample preparation, a small amount of the solid was pressed to the inner wall of a self-made low temperature quartz cuvette with a spatula until the glass was covered with a thin layer of the sample. The measurements were carried out in a liquid nitrogen cooled cryostat Optistat DN from *Oxford Instruments*.

fs-Transient absorption experiments were conducted using a Helios-Fire pump-probe setup from *Ultrafast Systems* paired with a regeneratively amplified 1030 nm laser (Pharos, *Light Conversion*, 1030 nm, 200 fs, 200 µJ). The effective laser repetition rate of 1 kHz was set via an internal pulse picker. A small portion of the 1030 nm fundamental was directed to the optical delay line and was subsequently used to generate broadband probe light by focusing the beam onto a sapphire (Vis/NIR range) or CaF_2 (UV/Vis range) crystal. The pump pulse was generated with an optical parametric amplifier (Orpheus-F, *Light Conversion*). The samples were measured in a 1 mm quartz cuvette under argon. To cover the whole spectral region from 350 nm to 900 nm, the UV/Vis and Vis/NIR part of the transient absorption spectra were recorded separately under identical conditions and were combined using the overlap of both datasets in the vis region (500 nm – 550 nm). The software Glotaran 1.5.1 was employed for the global analysis of the TA data.[4]

Photolysis experiments were conducted under argon in airtight quartz cuvettes (1 cm) with $[Mn(dgpy)_2][PF_6]_4$ (50 µM) in dry solvents and in the absence or presence of the substrates given. The high-power LEDs UHP-T-730-LA34 (730 nm, 2.6 W) and UHP-T-850-LA33 (850 nm, 5.1 W) from *Prizmatix* were employed as collimated light sources (for emission spectra, see Supplementary Figs. 2 and 3).[5] The temperature of the solution was kept constant at 25 °C using an *Agilent* Cary single cell peltier. To monitor the reaction progress, UV/Vis/NIR absorption spectra were recorded at regular time intervals. Supplementary Fig. 1 shows a representative photolysis experiment with irradiation at 730 nm.

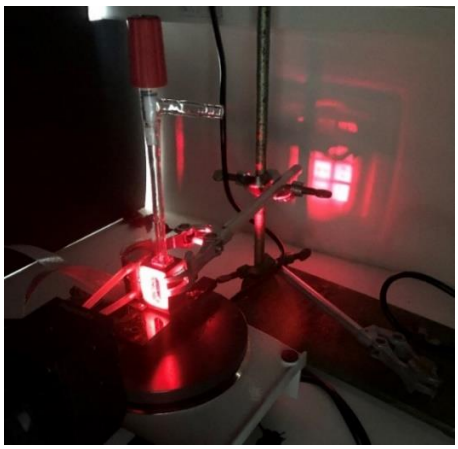

Figure 1. Photolysis experiment with the 730 LED.

ESI mass spectra were recorded directly from the photolysis reaction without further workup. Samples for HPLC quantification were treated with water (1 ml) and left to stand for 12 h at ambient conditions to give a brown precipitate (likely MnO_2). After filtration, the solvents were removed under reduced pressure and the yellow residue was dissolved in CH_3CN and subjected to HPLC.

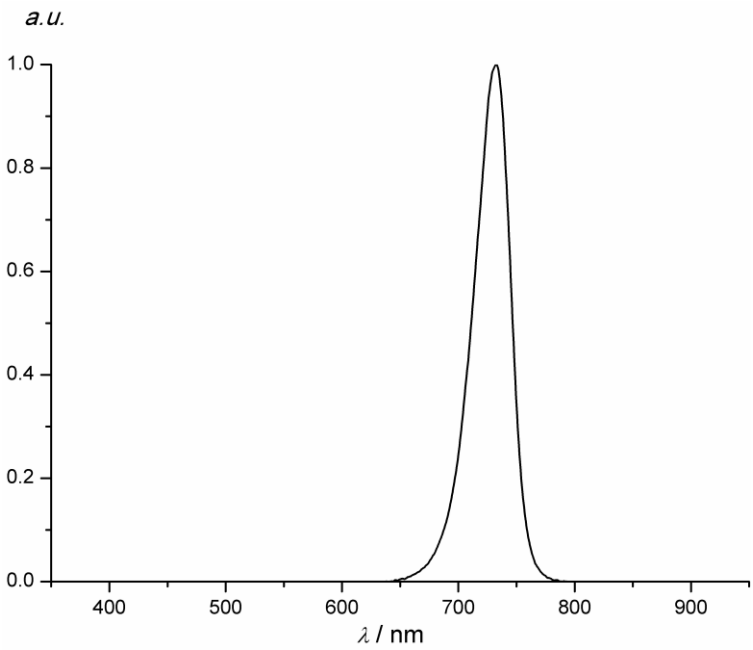

Figure 2. Normalized emission spectrum of the Prizmatix UHP-T-LA-730 LED series Ultra High Power LED (730 nm).[5]

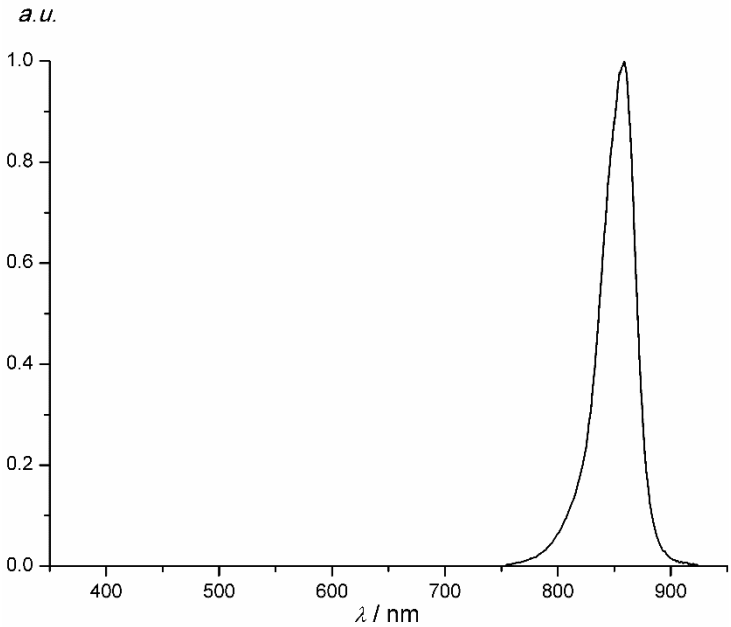

Figure 3. Normalized emission spectrum of the Prizmatix UHP-T-LA-850 LED series Ultra High Power LED (850 nm).[5]

Density Functional Theory (DFT) calculations were carried out using the ORCA program package[6] (version 5.0.1). Tight convergence criteria were chosen for all calculations (keywords *tightscf* and *tightopt*). All calculations were performed using the B3LYP functional[7–9] employing the RIJCOSX approximation (keyword *RIJCOSX*).[10,11] Relativistic effects were calculated at the zeroth order regular approximation (keyword *ZORA*) level.[12] The *ZORA* keyword automatically invokes relativistically adjusted basis sets. To account for solvent effects, a conductor-like screening model (keyword *CPCM*) modeling acetonitrile was used in all calculations.[13,14] Geometry optimizations were performed using Ahlrichs' polarized valence triple-zeta basis set (def2-TZVPP).[15,16] Atom-pairwise dispersion correction was performed with the Becke-Johnson damping scheme (D3BJ).[17,18] The energy of the electronic states and presence of energy minima were checked by numerical frequency calculations. Explicit counter ions and/or solvent molecules were not taken into account. The charge transfer number analyses of the time-dependent DFT (TDDFT)-calculated transitions were done using TheoDORE 2.2.[19,20]

Molecular dynamics simulations were performed using the GROMACS 2018.4 program package employing the (optimized potentials for liquid simulations - all atom) OPLS-AA force field.[21,22] All topologies were generated by hand. The geometry of the $[Mn(dgpy)_2]^{4+}$ ion was used as computed quantum chemically.[2] Mulliken charges were generated from a single point UHF calculation with a 6-31G basis using the Q-Chem 5.3.2 program package.[23] For the short-range interactions a cut-off of 1.2 nm was used and the long-range Coulomb interaction was treated using the particle-mesh Ewald method,[24] while for the van der Waals interaction a dispersion correction was applied.[5] Periodic boundary conditions were used and the time step was 2 fs, which was possible because all bonds including a hydrogen atom were restrained to their equilibrium value using the LINCS algorithm.[26] The production run was prepared according to the following protocol. After an energy minimization of the solvated system, consisting of the complex, four $[PF_6]^-$ ions and 1760 acetonitrile molecules, an equilibration of 1 ns in the NVT ensemble at T = 298 K was performed using a velocity rescaling thermostat[27] with a time constant of 0.1 ps. Afterwards, the system was simulated for 1 ns in the NPT ensemble at a pressure of 1 bar using a Berendsen barostat[28] with a time constant of 2 ps and an isothermal compressibility of 1.26×10^{-4} bar^{-1} yielding a box size of $(5.43\ nm)^3$. The system was then simulated at equilibrium for 1 µs and the resulting trajectory was analyzed using the tools provided by the GROMACS program package.

Synthesis of $[Mn(dgpy)_2][ClO_4]_4$: A solution of 50 mg (0.034 mmol, 1.0 eq) $[Mn(dgpy)_2][PF_6]_4$ [2] in dry CH_3CN (3 mL) was added to a solution of 116 mg (0.34 mmol, 10 eq) $[^nBu_4N][ClO_4]$ in dry CH_3CN (2 mL). The reaction was stirred at ambient temperature for 5 min. The product was purified by crystallization via slow diffusion of dry diethyl ether into a concentrated solution in acetonitrile to yield dark crystals. To ensure complete anion exchange, this procedure was repeated with another 10 eq of $[^nBu_4N][ClO_4]$ to yield dark crystals of $[Mn(dgpy)_2][ClO_4]_4$. The absence of $[PF_6]^-$ (831 and 558 cm^{-1}) and the presence of $[ClO_4]^-$ (1075, 1042 and 1010 cm^{-1}) was confirmed by IR spectroscopy (Figure 4). IR (ATR): $\tilde{\upsilon}$ / cm^{-1} = 1576 (s), 1486(m), 1460 (m, sh), 1435 (m, sh), 1407 (w), 1380 (s), 1153 (w), 1075 (s), 1042 (s, sh), 1010 (s, sh), 938 (w, sh), 910 (m), 880 (m, sh), 848 (w), 800 (m), 749 (w, sh), 735 (m), 707(m).

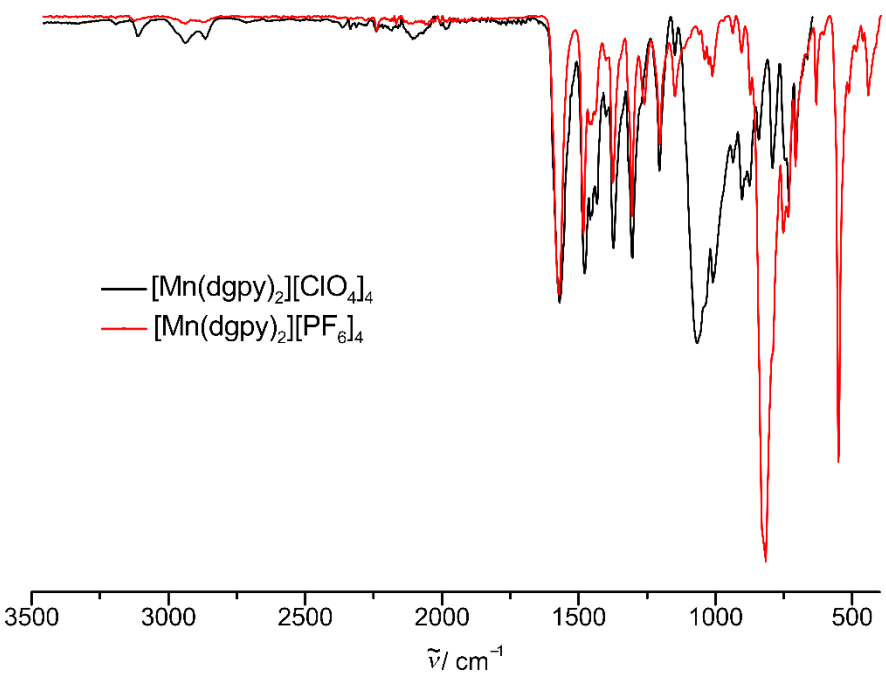

Figure 4. ATR-IR spectra of $[Mn(dgpy)_2][PF_6]_4$ (red) and $[Mn(dgpy)_2][ClO_4]_4$ (black) showing the successful $[PF_6]^-$ to $[ClO_4]^-$ counter ion exchange.

2. Analytical and Spectroscopic Data

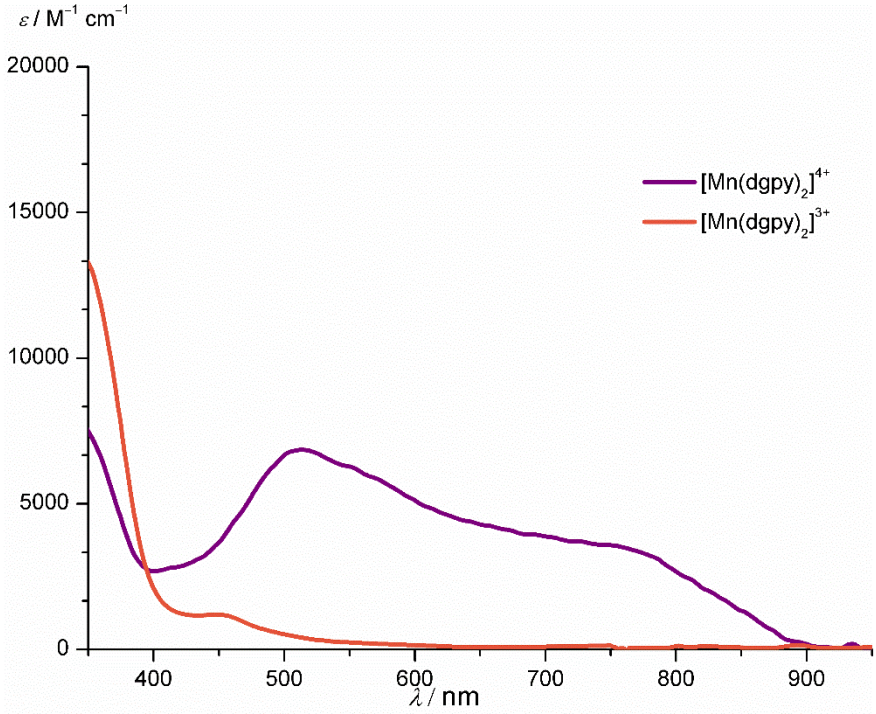

Figure 5. Absorption spectra of $[Mn(dgpy)_2][PF_6]_4$ (purple) and $[Mn(dgpy)_2][PF_6]_3$ (orange) in CH_3CN.[1]

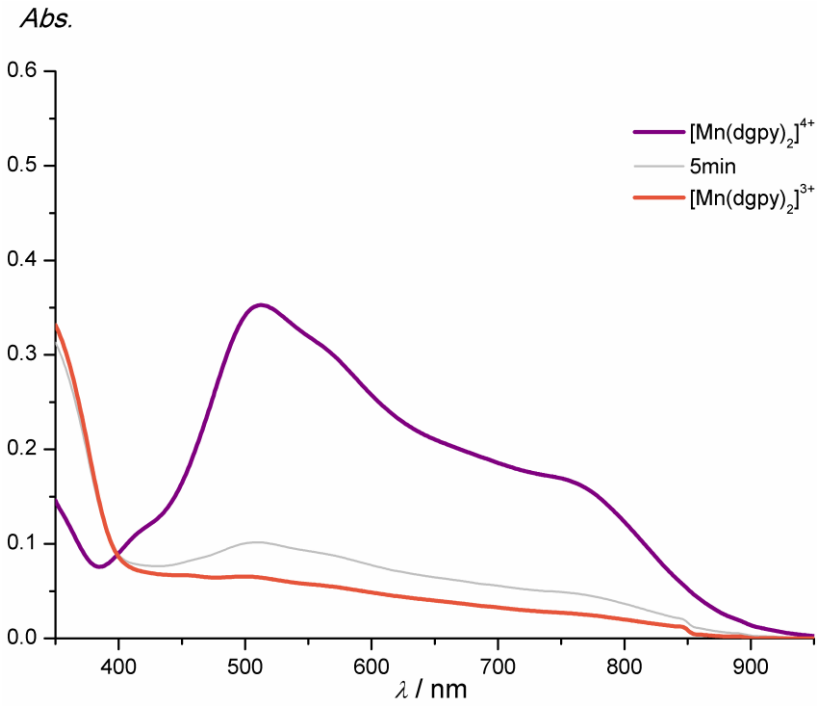

Figure 6. Absorption spectra of $[Mn(dgpy)_2][PF_6]_4$ (purple) and after addition of 1 eq $[n\text{-}Bu_4N]Cl$ in CH_3CN after 5 min (grey) and 10 min (orange) in the dark.

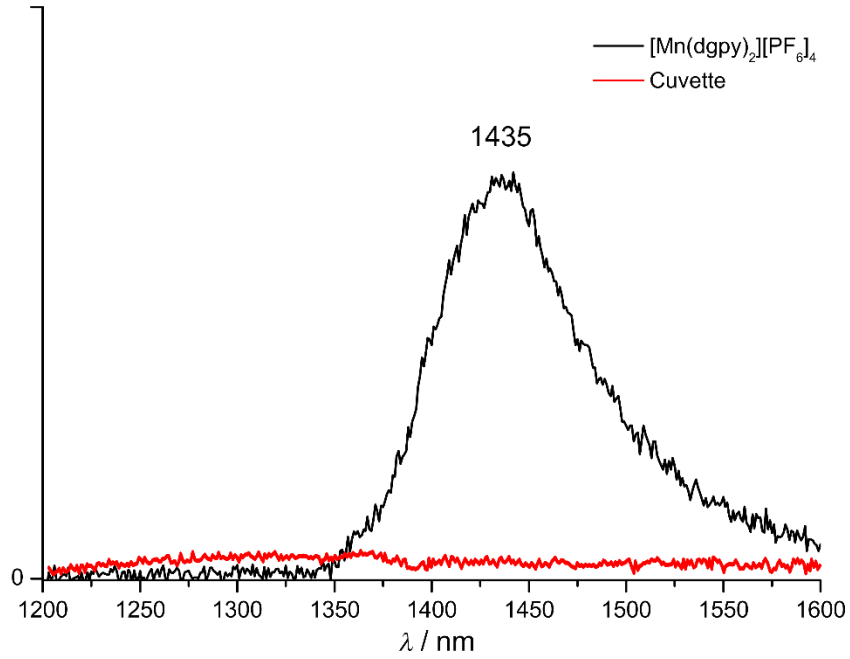

Figure 7. Luminescence spectra of $[Mn(dgpy)_2][PF_6]_4$ after laser excitation with 635 nm at 77 K with control measurement at 77 K (empty cuvette).

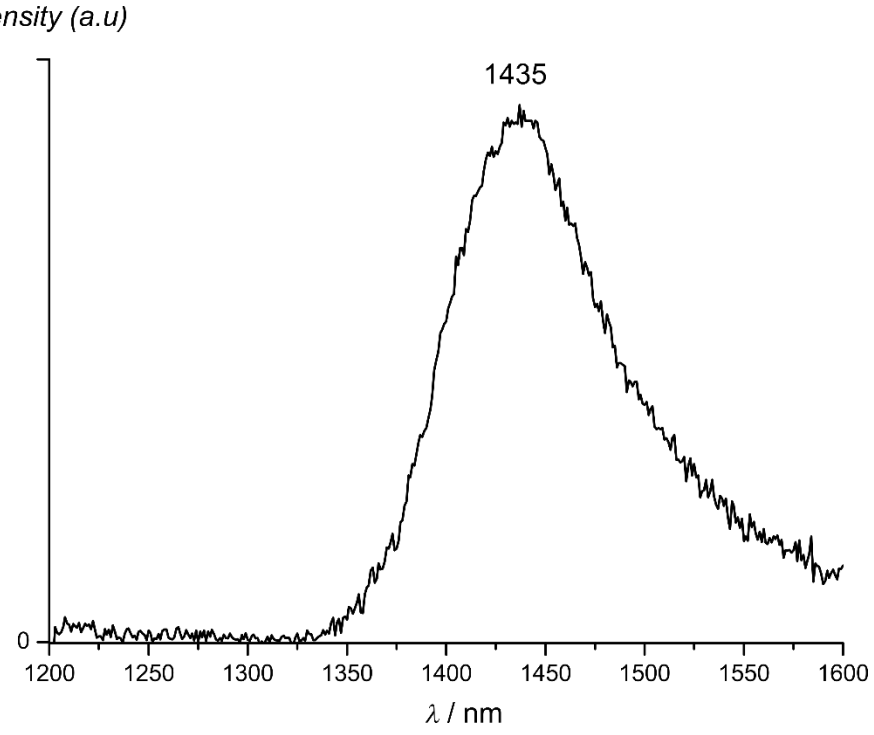

Figure 8. Luminescence spectra of $[Mn(dgpy)_2][PF_6]_4$ after laser excitation with 730 nm at 77 K.

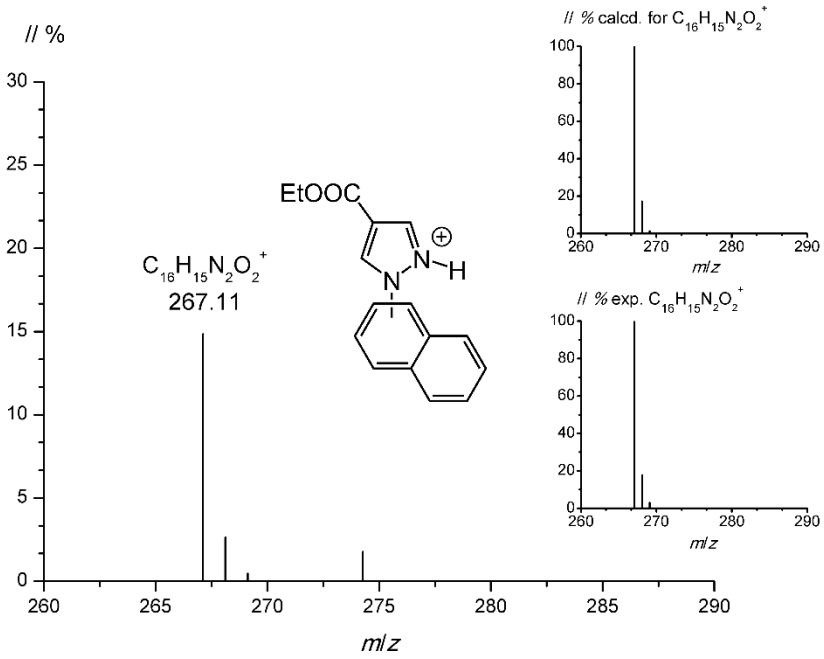

Figure 9. ESI$^+$ mass spectrum of the product generated from the oxidation of naphthalene $C_{10}H_8$ (0.3 M) in CH_3CN with $[Mn(dgpy)_2][PF_6]_4$ (2 mM) under 730 nm irradiation in the presence of 1H-pyrazole-4-carboxylic acid ethyl ester (30 mM). The inset shows the experimental and calculated isotopic patterns of the m/z = 267 ($[C_{16}H_{15}N_2O_2]^+$) peak.

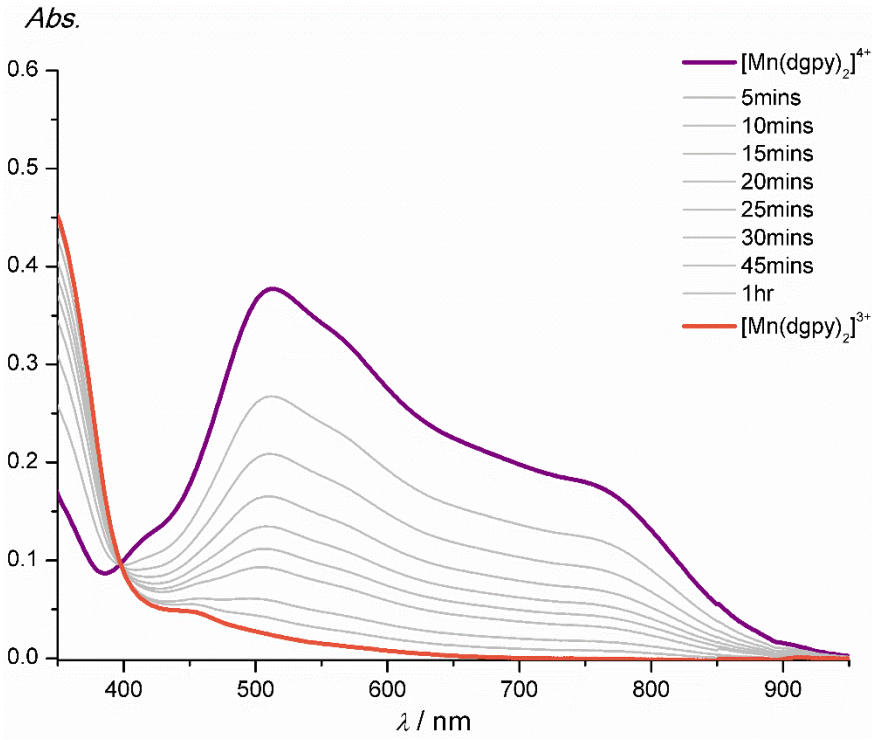

Figure 10. Absorption spectra of $[Mn(dgpy)_2][PF_6]_4$ (purple: before irradiation; orange: $[Mn(dgpy)_2][PF_6]_3$) during irradiation with the 730 nm LED in 0.3 M mesitylene in CH_3CN for 75 min.

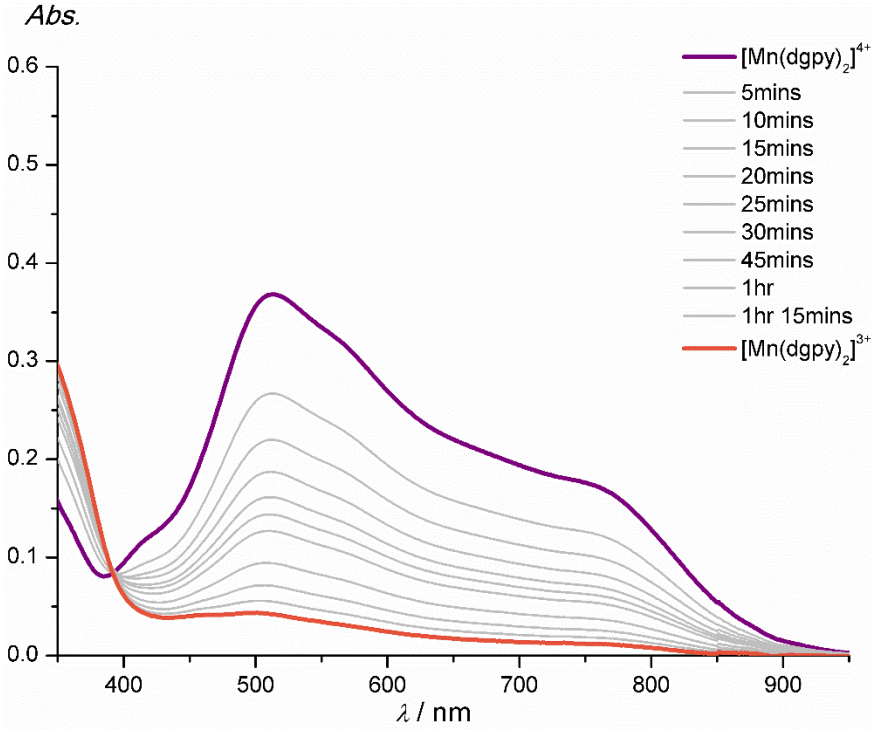

Figure 11. Absorption spectra of $[Mn(dgpy)_2][PF_6]_4$ (purple: before irradiation; orange: $[Mn(dgpy)_2][PF_6]_3$) during irradiation with the 730 nm LED in 0.3 M toluene in CH_3CN for 90 min.

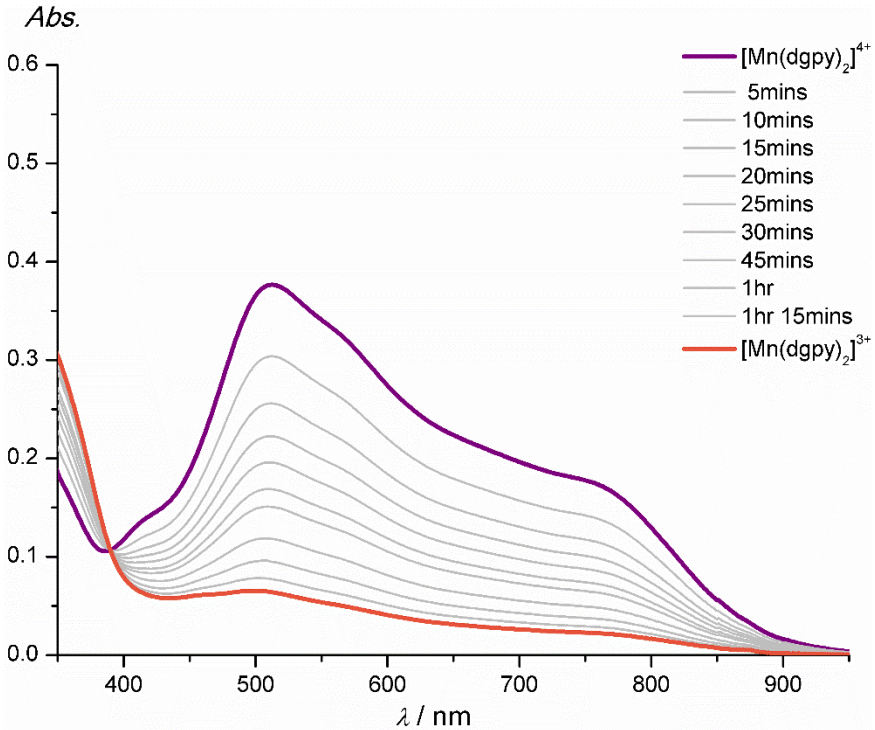

Figure 12. Absorption spectra of $[Mn(dgpy)_2][PF_6]_4$ (purple: before irradiation; orange: $[Mn(dgpy)_2][PF_6]_3$) during irradiation with the 730 nm LED in 0.3 M benzene in CH_3CN for 90 min.

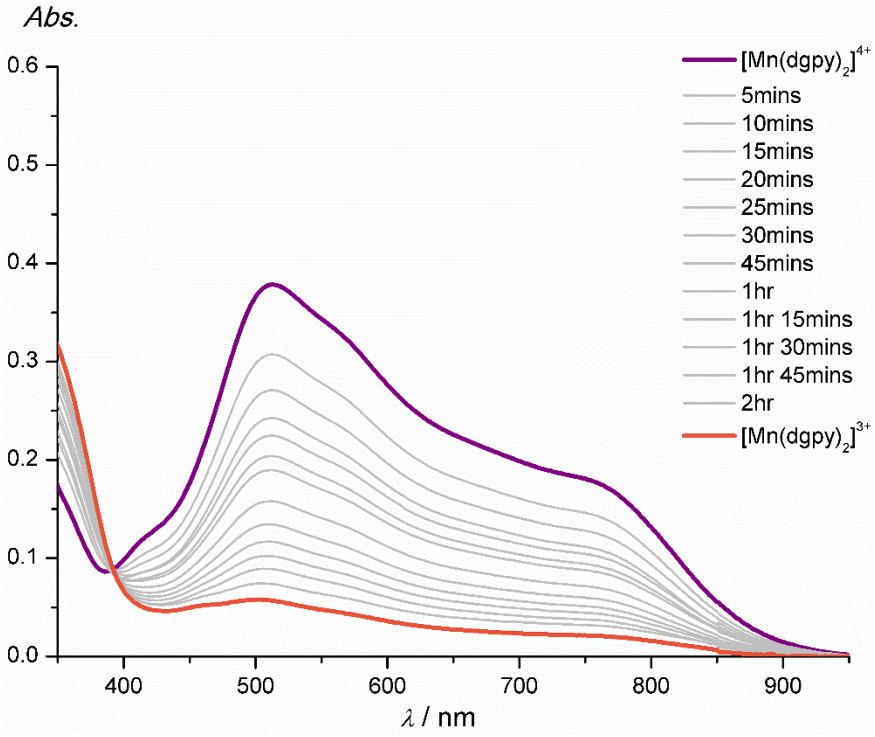

Figure 13. Absorption spectra of $[Mn(dgpy)_2][PF_6]_4$ (purple: before irradiation; orange: $[Mn(dgpy)_2][PF_6]_3$) during irradiation with the 730 nm LED in CH_3CN for 135 min.

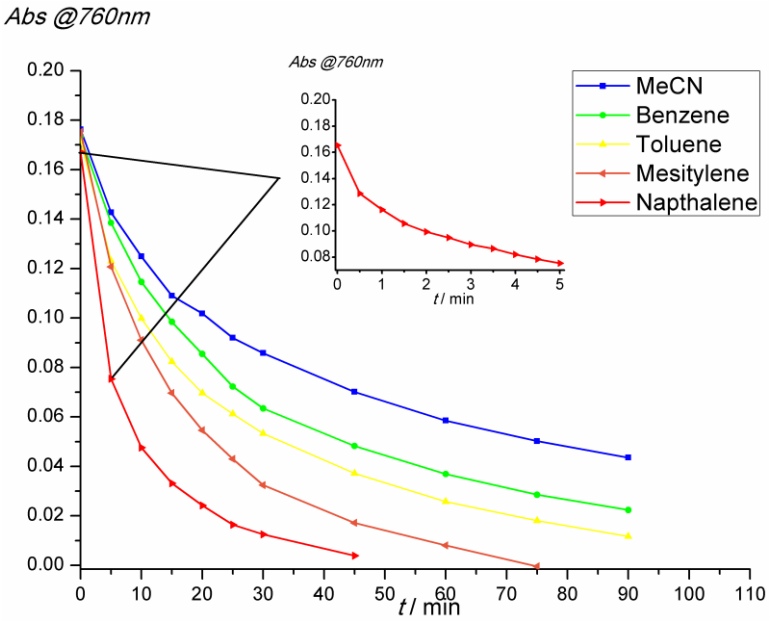

Figure 14. Kinetic traces observed at 760 nm of $[Mn(dgpy)_2][PF_6]_4$ under irradiation with 730 nm in CH_3CN (blue), 0.3 M benzene in CH_3CN (green), 0.3 M toluene in CH_3CN (yellow), 0.3 M mesitylene in CH_3CN (orange) and 0.3 M naphthalene in CH_3CN (red). The inset shows the reaction with naphthalene over a minute time scale, measured in a separate experiment, demonstrating the high initial rate of this reaction.

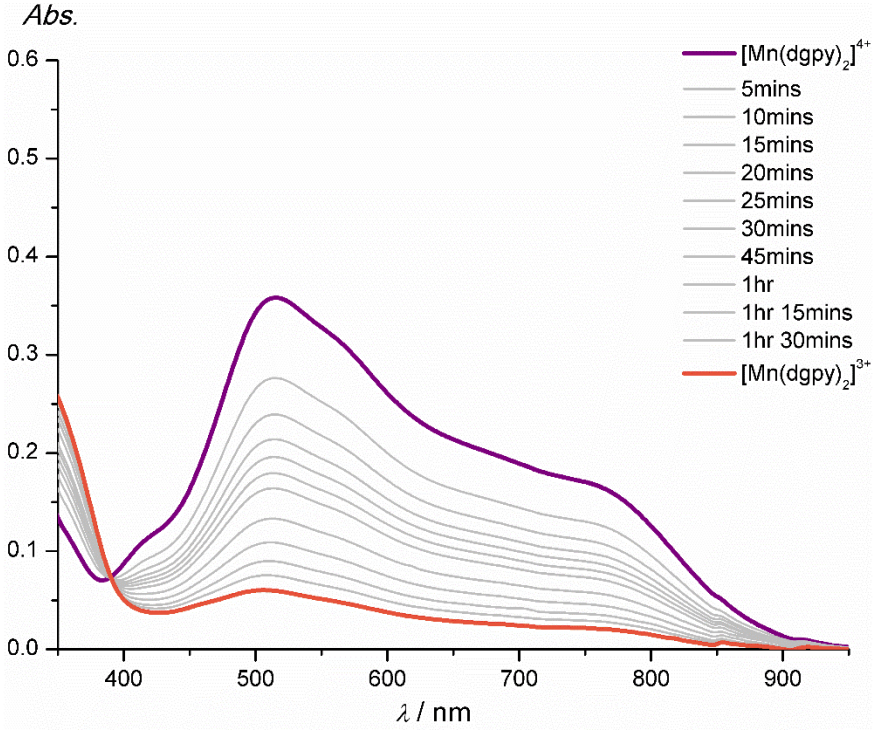

Figure 15. Absorption spectra of $[Mn(dgpy)_2][PF_6]_4$ (purple: before irradiation; orange: $[Mn(dgpy)_2][PF_6]_3$) during irradiation with the 730 nm LED in $CH_3CH_2CH_2CN$ for 105 min.

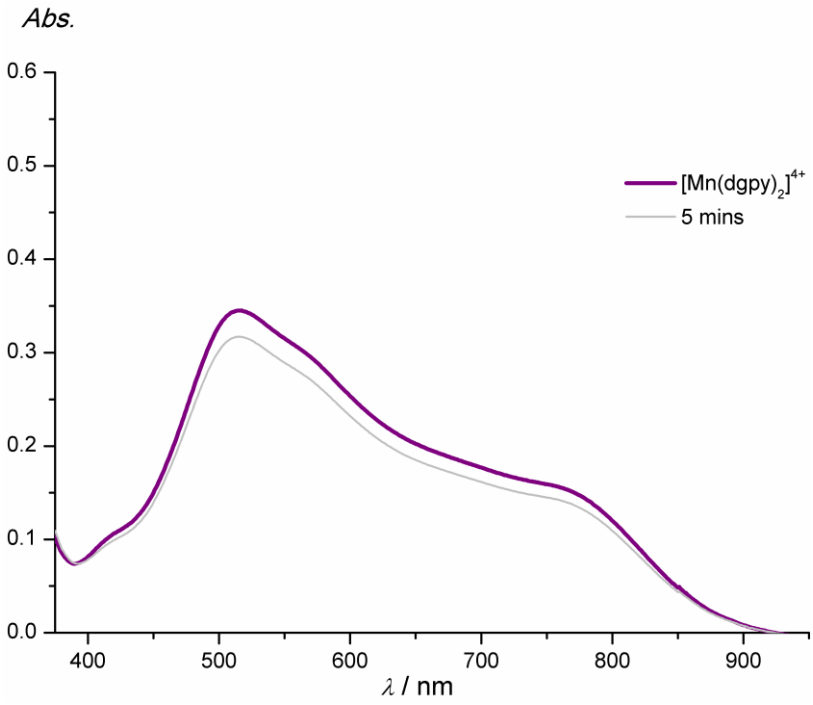

Figure 16. Absorption spectra of $[Mn(dgpy)_2][PF_6]_4$ (purple: before irradiation; grey: after 5 min irradiation) during irradiation with the 730 nm LED in CH_3NO_2.

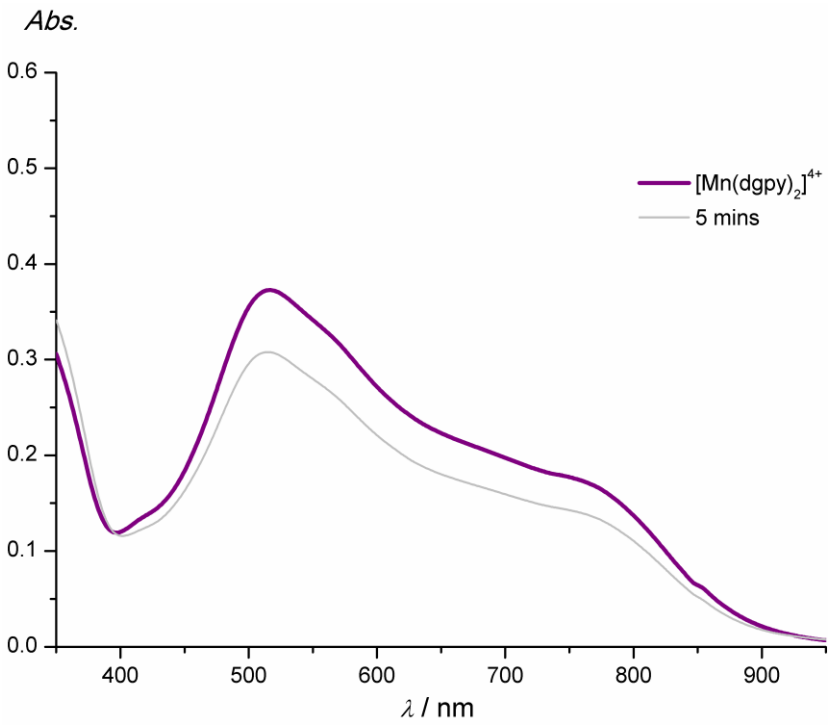

Figure 17. Absorption spectra of $[Mn(dgpy)_2][PF_6]_4$ (purple: before irradiation; grey: after 5 min irradiation) during irradiation with the 730 nm LED in 1,2-butylene carbonate.

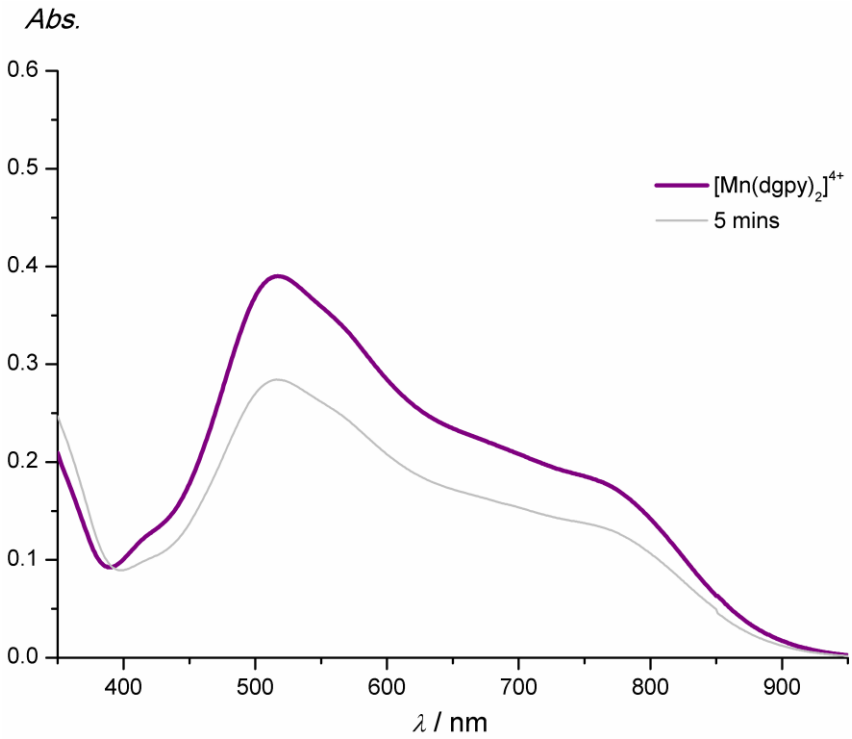

Figure 18. Absorption spectra of $[Mn(dgpy)_2][PF_6]_4$ (purple: before irradiation; orange: grey 5 min irradiation) during irradiation with the 730 nm LED in γ-valerolactone.

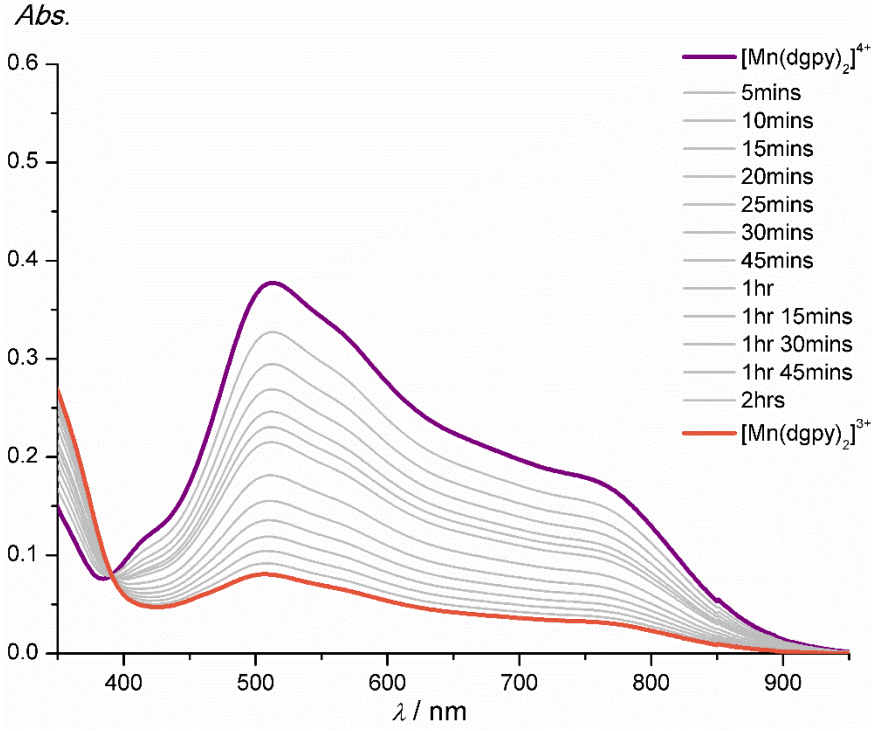

Figure 19. Absorption spectra of $[Mn(dgpy)_2][PF_6]_4$ (purple: before irradiation; orange: $[Mn(dgpy)_2][PF_6]_3$) during irradiation with the 850 nm LED in CH_3CN for 135 min.

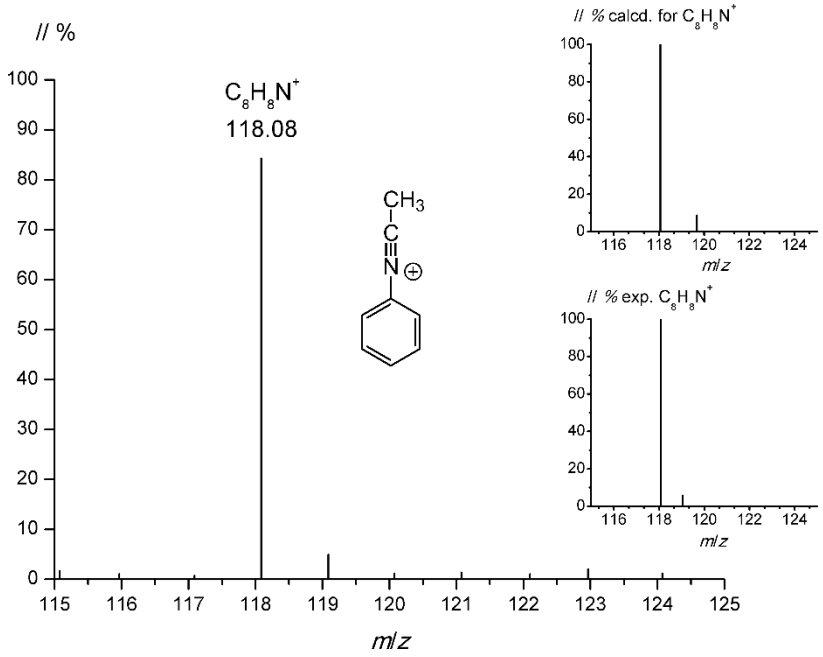

Figure 20. ESI^+ mass spectrum of the nitrilium product generated from the oxidation of benzene C_6H_6 (0.3 M) in CH_3CN with $[Mn(dgpy)_2][PF_6]_4$ (1 mM) under 730 nm irradiation. The inset shows the experimental and calculated isotopic pattern of the m/z = 118 peak ($[C_8H_8N]^+$).

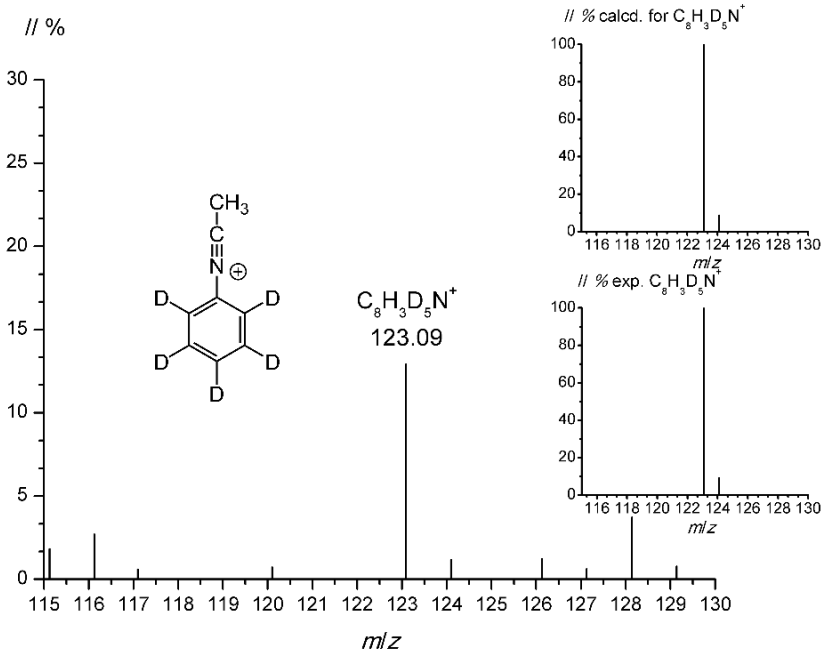

Figure 21. ESI^+ mass spectrum of the nitrilium product generated from the oxidation of deuterated benzene C_6D_6 (0.3 M) in CH_3CN with $[Mn(dgpy)_2][PF_6]_4$ (1 mM) under 730 nm irradiation. The inset shows the experimental and calculated isotopic pattern of the m/z = 123 peak ($[C_8H_3D_5N]^+$).

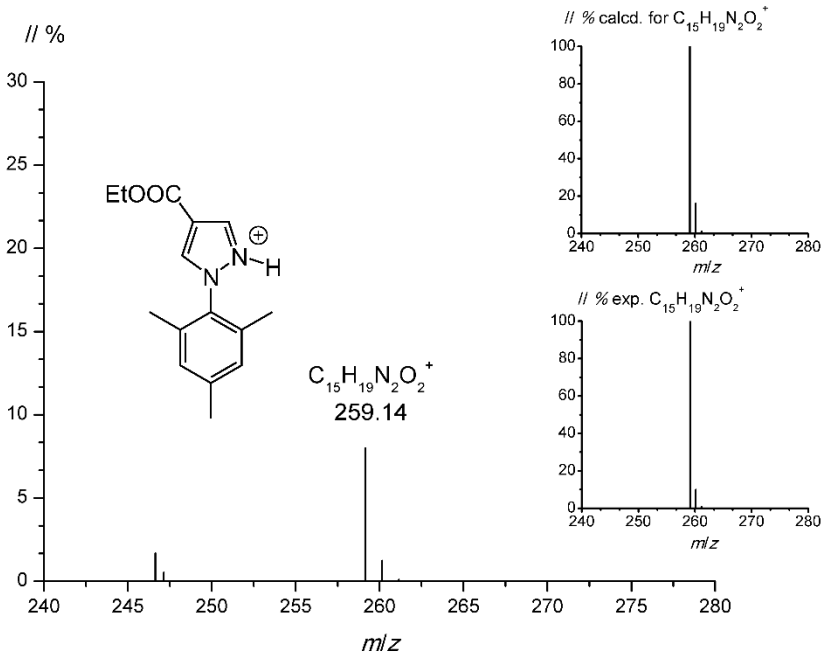

Figure 22. ESI^+ mass spectrum of the product generated from the oxidation of mesitylene (15 mM) in CH_3CN with $[Mn(dgpy)_2][PF_6]_4$ (4.5 mM) under 730 nm irradiation in the presence of 1H-pyrazole-4-carboxylic acid ethyl ester (15 mM). The inset shows the experimental and calculated isotopic pattern of the *m/z* = 259 peak ($[C_{15}H_{19}N_2O_2]^+$).

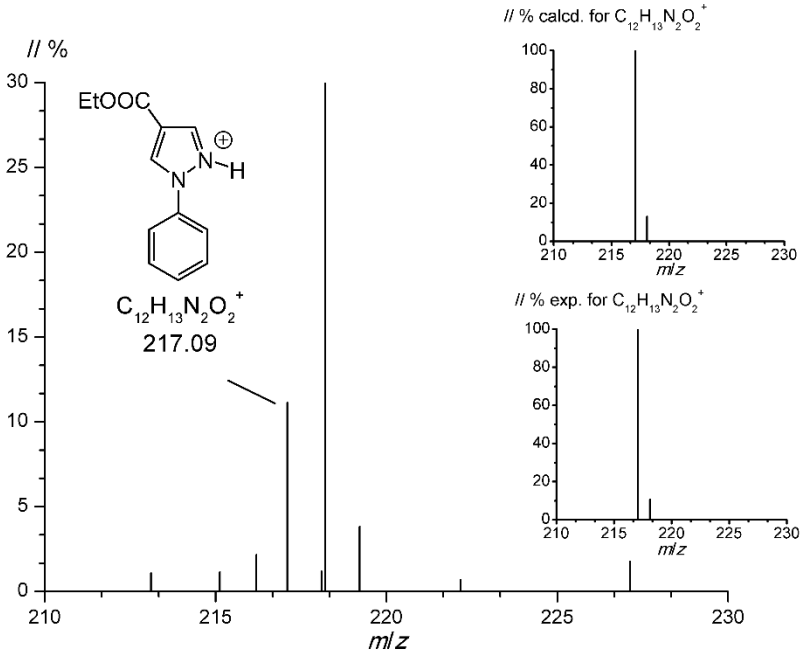

Figure 23. ESI^+ mass spectrum of the product generated from the oxidation of benzene C_6H_6 (1.3 M) in CH_3CN with $[Mn(dgpy)_2][PF_6]_4$ (2 mM) under 730 nm irradiation in the presence of 1H-pyrazole-4-carboxylic acid ethyl ester (30 mM). The inset shows the experimental and calculated isotopic patterns of the *m/z* = 217 ($[C_{12}H_{13}N_2O_2]^+$) peak.

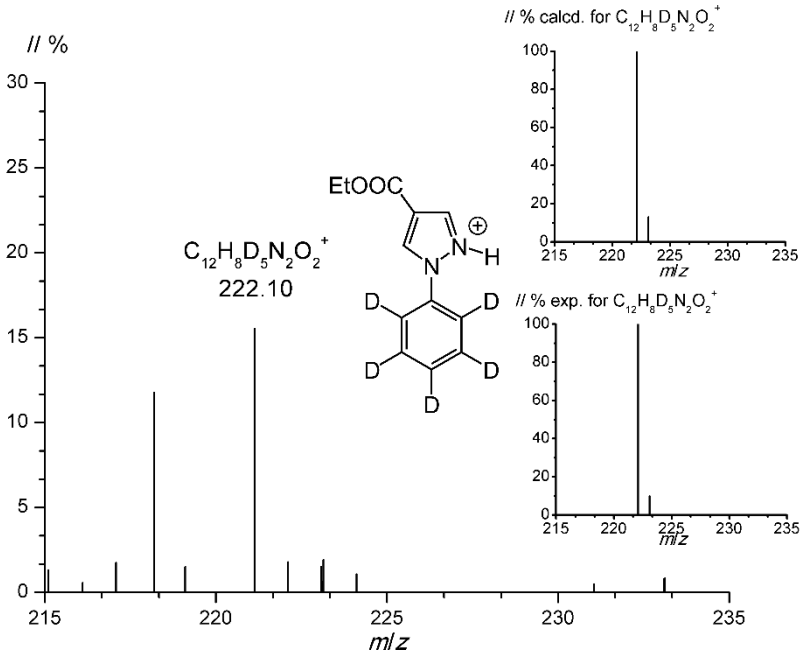

Figure 24. ESI^+ mass spectrum of the product generated from the oxidation of deuterated benzene C_6D_6 (1.3 M) in CH_3CN with $[Mn(dgpy)_2][PF_6]_4$ (2 mM) under 730 nm irradiation in the presence of 1H-pyrazole-4-carboxylic acid ethyl ester (30 mM). The inset shows the experimental and calculated isotopic patterns of the *m/z* = 222 ($[C_{12}H_8D_5N_2O_2]^+$) peak.

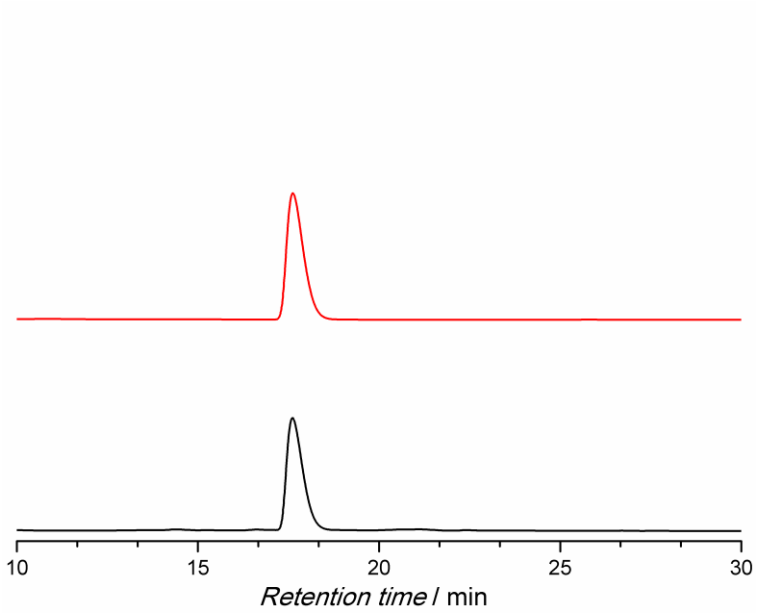

Figure 25. HPLC chromatogram of an authentic sample of ethyl 1-phenyl-1H-pyrazole-4-carboxylate as reference in CH_3CN/H_2O (red) and of the product of the 730 nm photolysis of benzene (1.3 M), 1H-pyrazole-4-carboxylic acid ethyl ester (30 mM) and $[Mn(dgpy)_2][PF_4]_4$ (4.5 mM) as limiting reagent in CH_3CN. Yield (11 %) determined by comparison of peak areas.

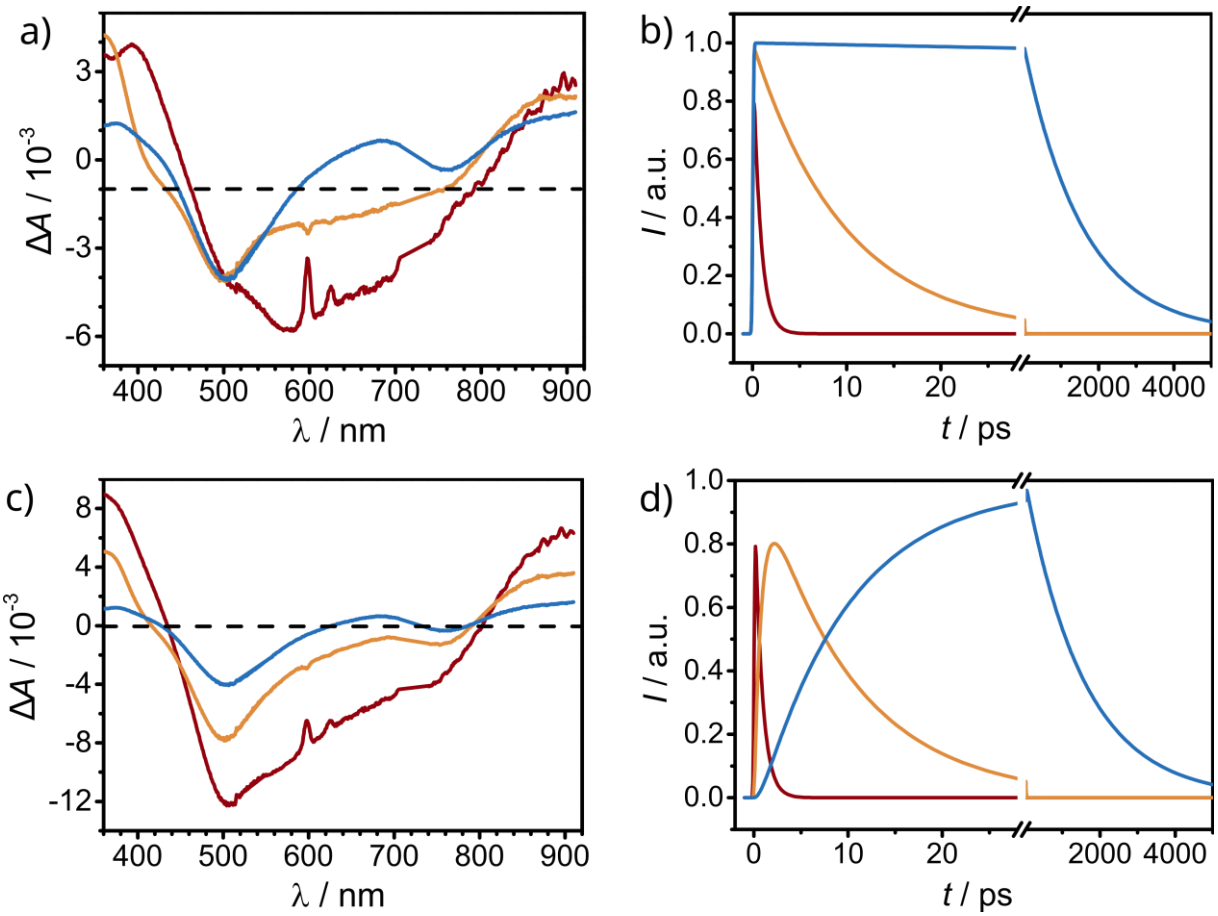

Figure 26. a) Decay associated difference spectra and c) evolution associated difference spectra and corresponding decay traces b) and d) of the global fit of the TA spectra obtained upon 730 nm excitation (800 nJ / pulse) of $[Mn(dgpy)_2][PF_6]_4$ in CH_3CN (Fig. 2a of the main article). Lifetimes: 780 fs (red), 9.7 ps (orange), 1.6 ns (blue).

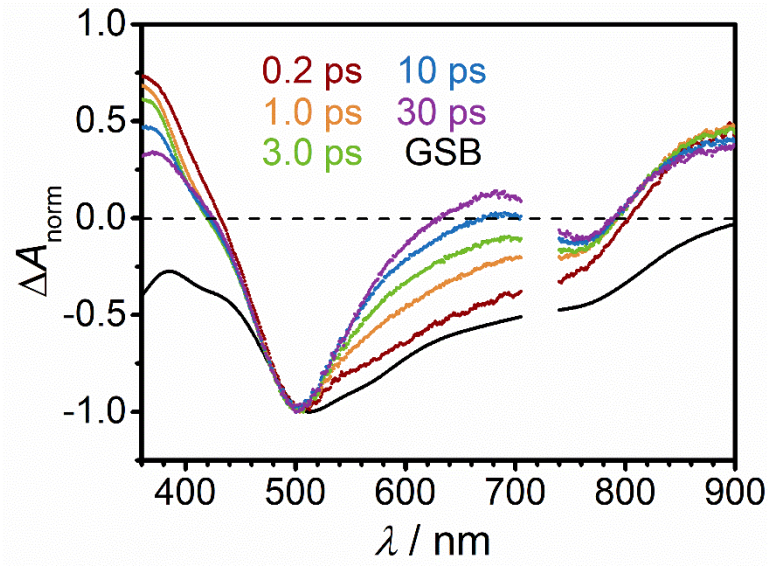

Figure 27. Normalized fs-transient absorption spectra of $[Mn(dgpy)_2][PF_6]_4$ in CH_3CN after laser excitation at 730 nm (800 nJ / pulse) and hypothetical ground state bleach spectrum obtained from the normalized negative ground state spectrum of $[Mn(dgpy)_2][PF_6]_4$ in CH_3CN (black).

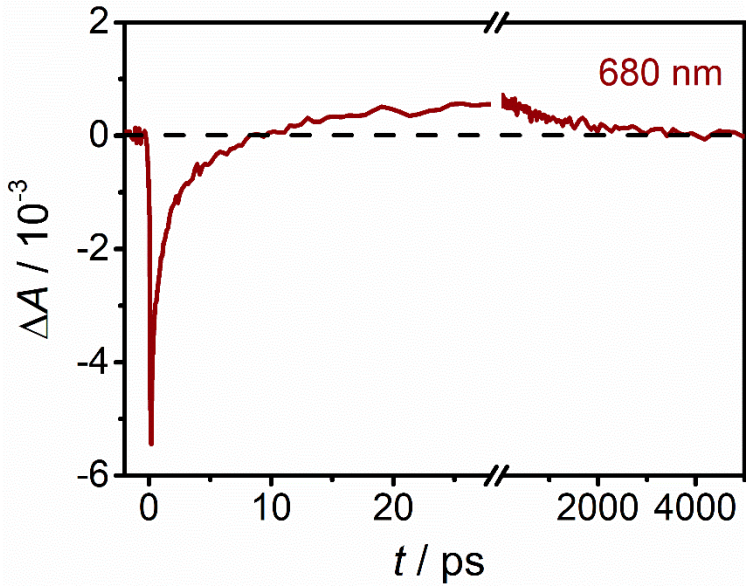

Figure 28. Decay trace at 680 nm from the transient absorption spectra of $[Mn(dgpy)_2][PF_6]_4$ in CH_3CN after excitation with 730 nm laser pulses (800 nJ / pulse)

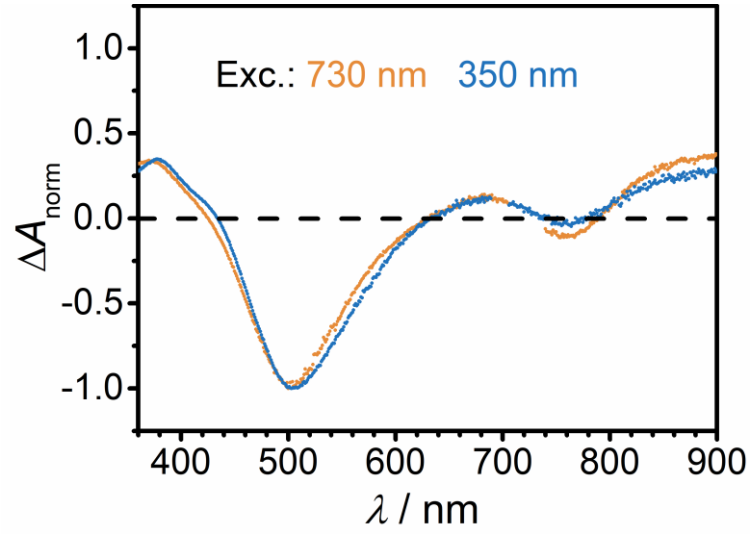

Figure 29. Normalized fs-transient absorption spectra of $[Mn(dgpy)_2][PF_6]_4$ in CH_3CN 30 ps after laser excitation at 350 nm (400 nJ / pulse, blue) and 730 nm (800 nJ / pulse, orange), respectively.

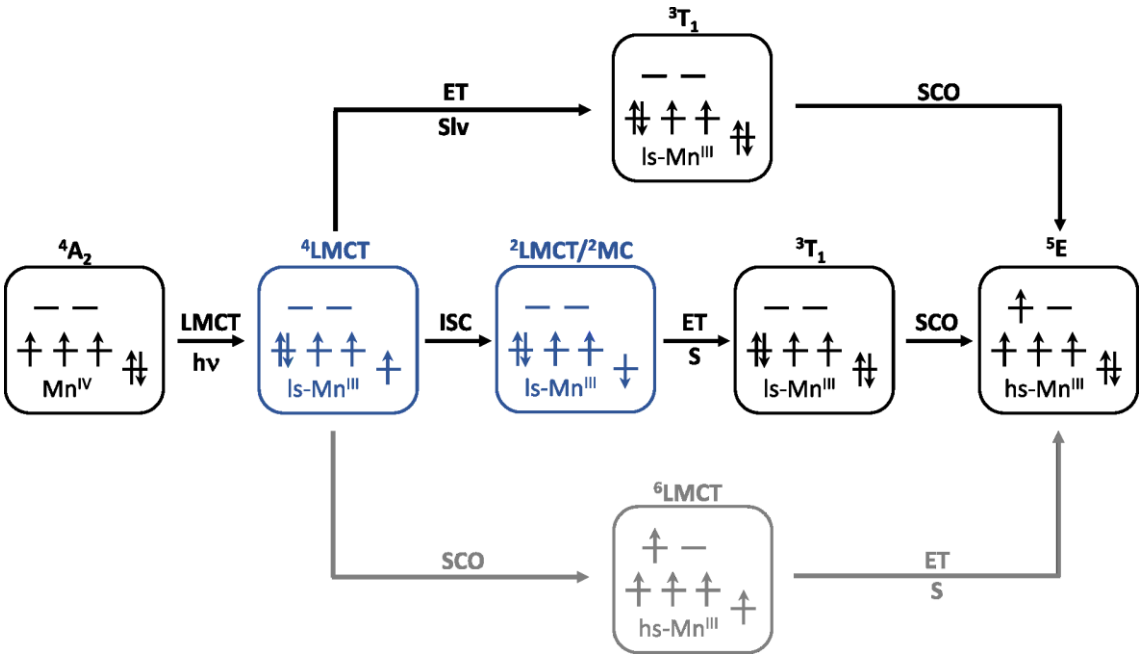

Figure 30. Possible mechanistic scenarios of the dynamics of the ^{4}LMCT excited state by static quenching by hole transfer to a solvent molecule Slv (top), by ISC to the ^{2}LMCT/^{2}MC state followed by hole transfer to a substrate (e.g. naphthalene as shown in the main text) to given the low-spin manganese(III) complex ($^3T_1$) and SCO to the high-spin manganese(III) complex (^{5}E) (center) and SCO to give a ^{6}LMCT state followed by hole transfer to a substrate S (bottom) to give the high-spin manganese(III) complex (^{5}E). For details, see main article.

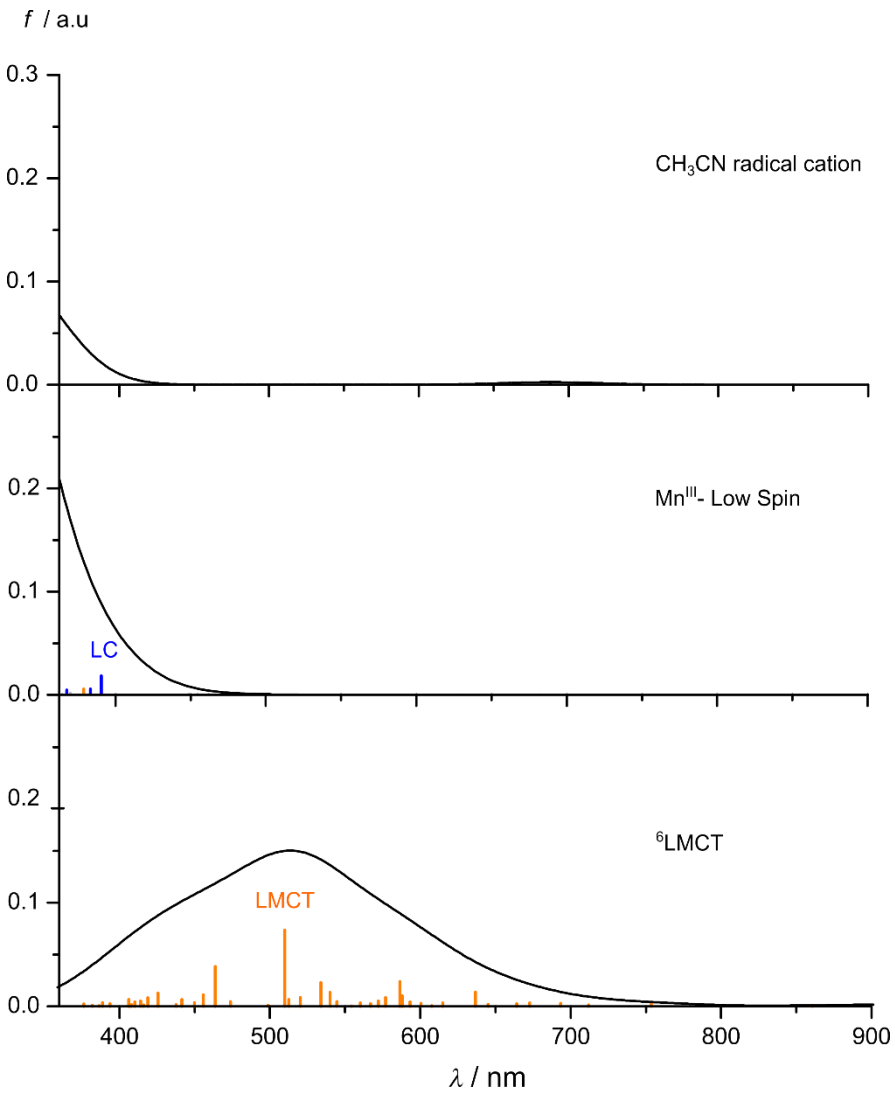

Figure 31. Time-dependent DFT calculated spin-allowed transitions of the CH_3CN radical cation in CH_3CN (top) of low-spin $[Mn(dgpy)_2]^{3+}$ ($^3T_1$) in CH_3CN (center) and of the ^{6}LMCT excited state of $[Mn(dgpy)_2]^{4+}$ (bootom). Color code of the stick spectra accordint to charge transfer number analysis (green: MLCT, purple: LLCT, orange: LMCT, blue: LC, gray: MC). Gaussian bands broadened with FWHM = 80 nm.

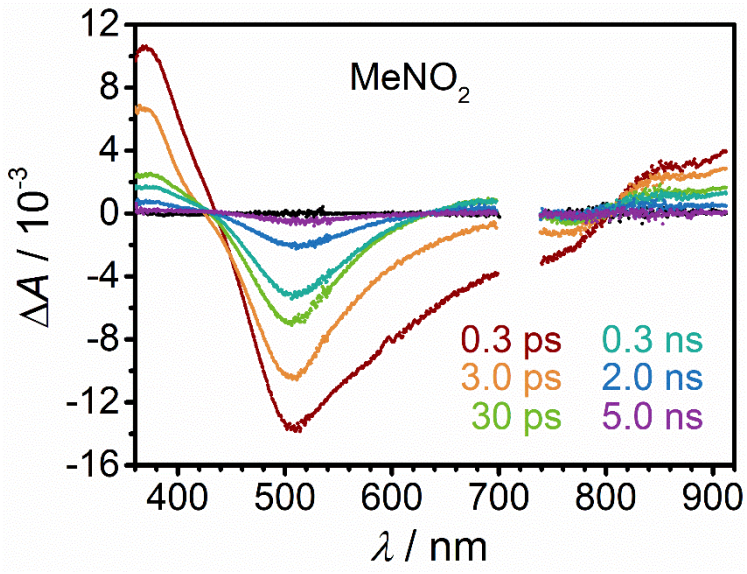

Figure 32. Transient absorption spectra of $[Mn(dgpy)_2][PF_6]_4$ in CH_3NO_2 after laser excitation at 730 nm (800 nJ / pulse).

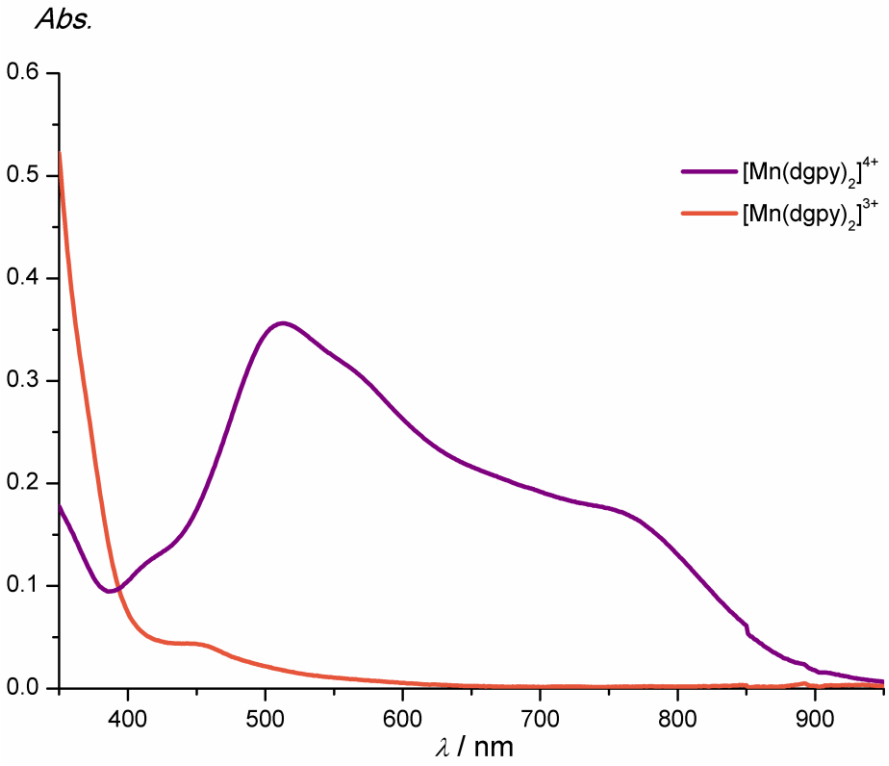

Figure 33. Absorption spectra of $[Mn(dgpy)_2][PF_6]_4$ (purple) and after addition of 1 eq dgpy (orange) in CH_3CN in the dark.

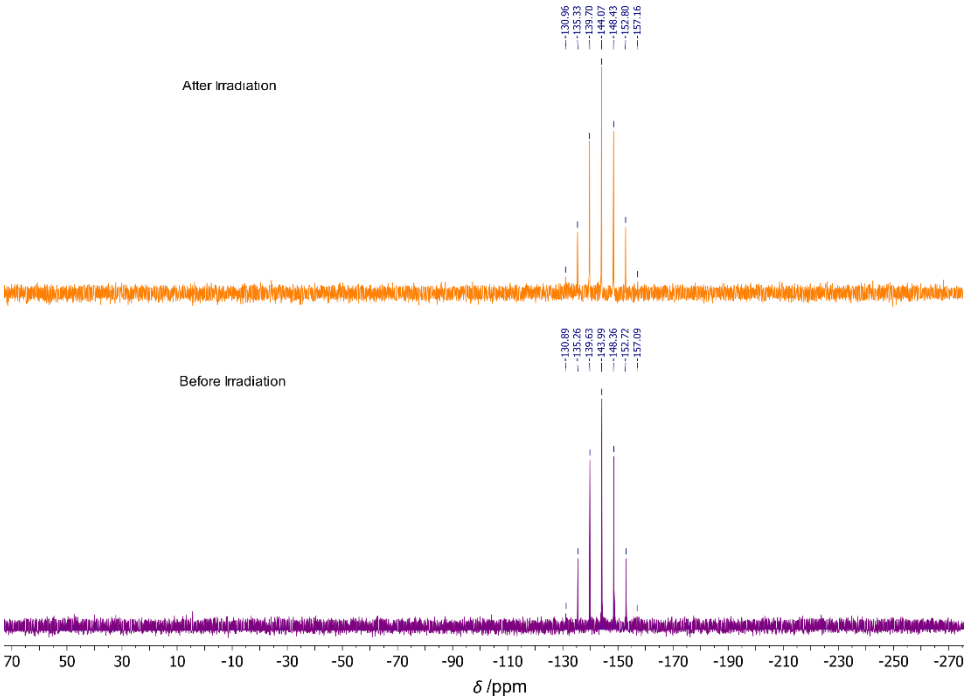

Figure 34. ^{31}P NMR spectra of $[Mn(dgpy)_2][PF_6]_4$ (top, purple: before irradiation; bottom, orange: after 120 min irradiation) during irradiation with the 730 nm LED in CD_3CN.

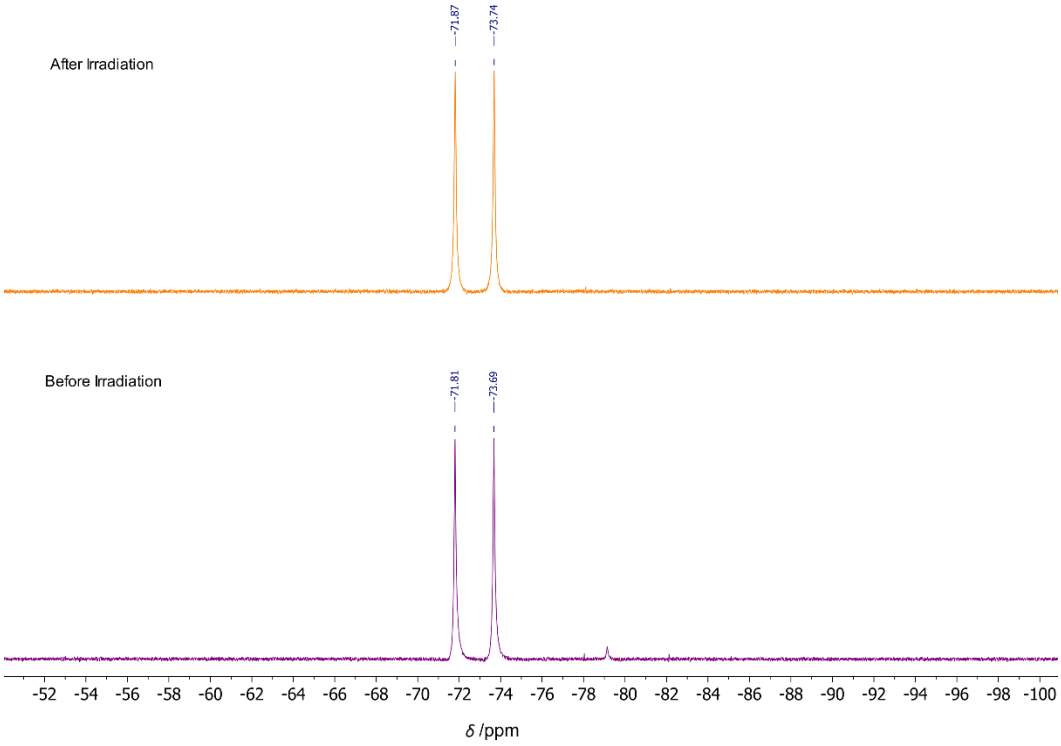

Figure 35. ^{19}F NMR spectra of $[Mn(dgpy)_2][PF_6]_4$ (top, purple: before irradiation; bottom, orange: after 120 min irradiation) during irradiation with the 730 nm LED in CD_3CN.

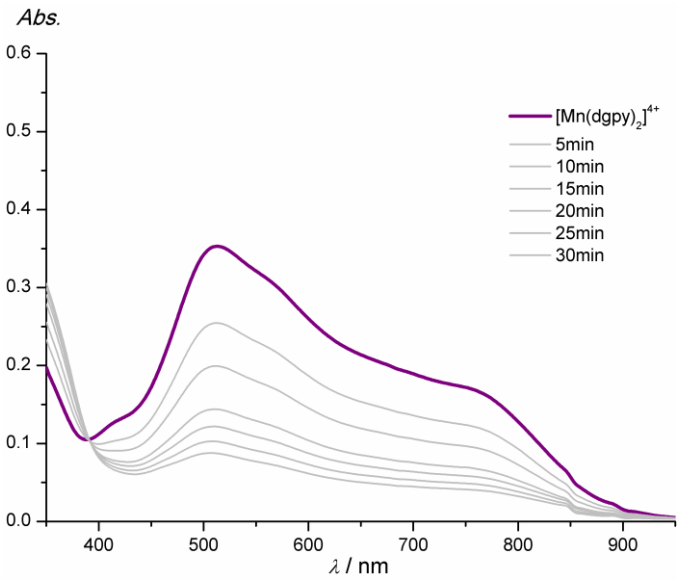

Figure 36. Absorption spectra of $[Mn(dgpy)_2][ClO_4]_4$ (purple: before irradiation) during 30 min irradiation with the 730 nm LED in CH_3CN.

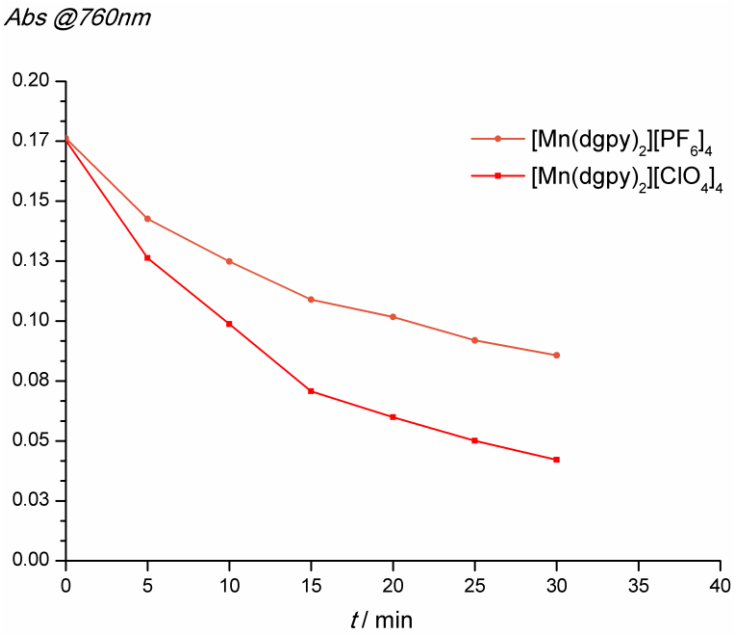

Figure 37. Kinetic traces observed at 760 nm of $[Mn(dgpy)_2][PF_6]_4$ (orange) and $[Mn(dgpy)_2][ClO_4]_4$ (red) under irradiation with 730 nm in CH_3CN.

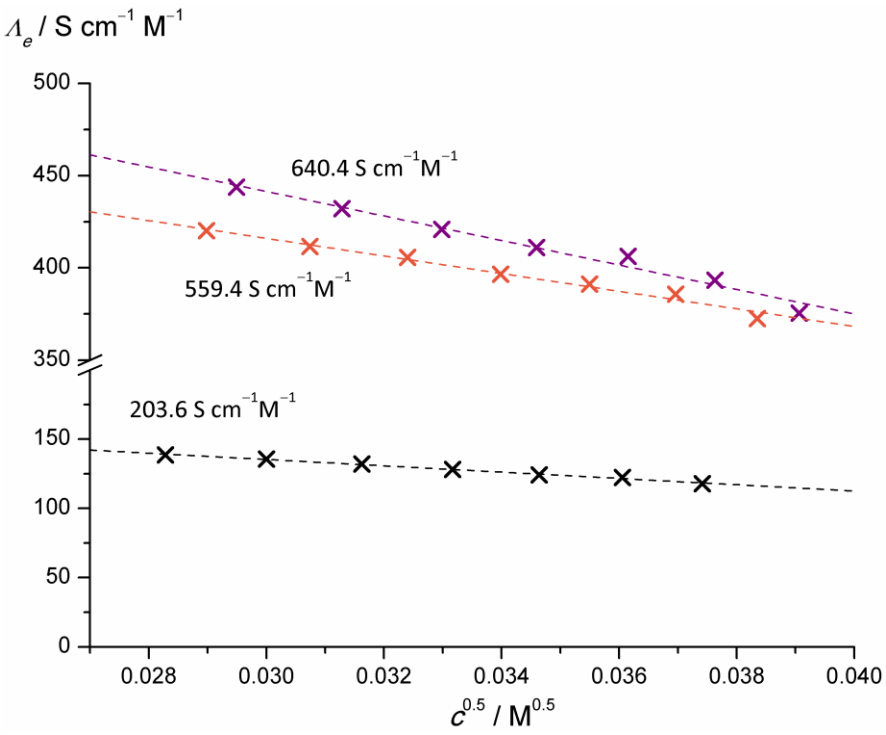

Figure 38. Equivalent conductivity Λ_e vs. $c^{1/2}$ plots of $[Mn(dgpy)_2][PF_6]_4$ (purple) $[Mn(dgpy)_2][PF_6]_4$ (orange) and $[n\text{-}Bu_4N][PF_6]$ (black) in CH_3CN at 293 K.

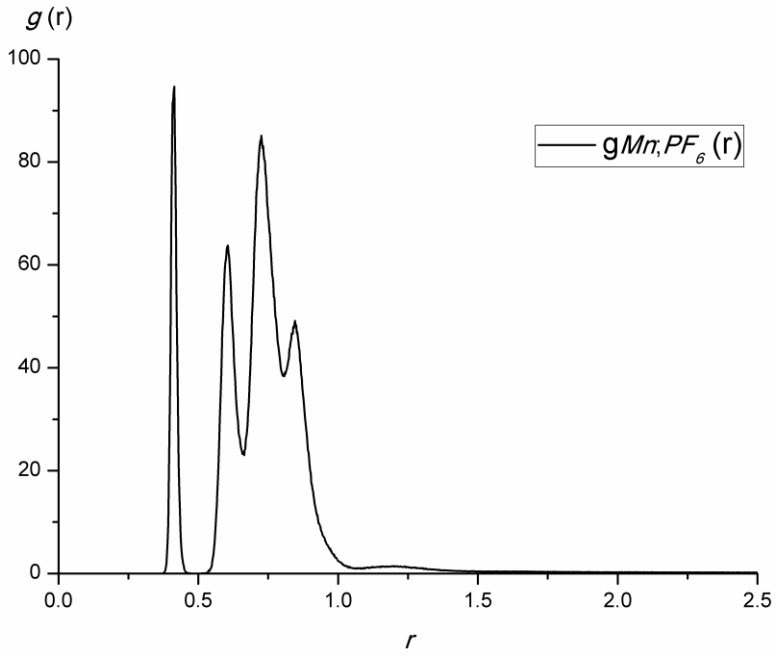

Figure 39. Radial distribution $g(r)$ of the four $[PF_6]^-$ counter ions (center of mass) from the Mn center in a molecular dynamics simulation of $[Mn(dgpy)_2][PF_6]_4$ in CH_3CN with maxima at 0.41, 0.61, 0.73 and 0.85 nm (sampling time 1 µs). The low number of $[PF_6]^-$ counter ions precludes a meaningful statistical analysis.

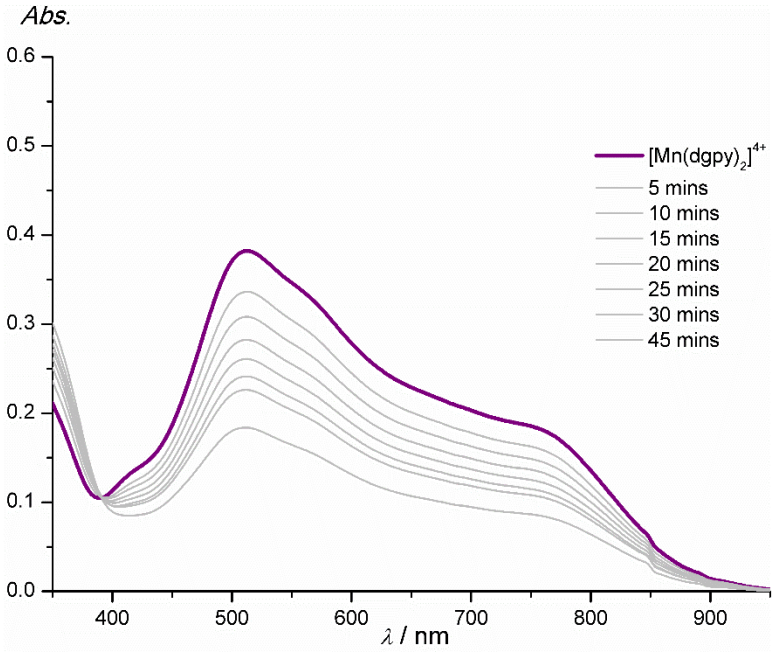

Figure 40. Absorption spectra of $[Mn(dgpy)_2][PF_6]_4$ in the presence of 50 mM $[n\text{-}Bu_4N][PF_6]$ (purple: before irradiation) during irradiation with the 730 nm LED in CH_3CN.

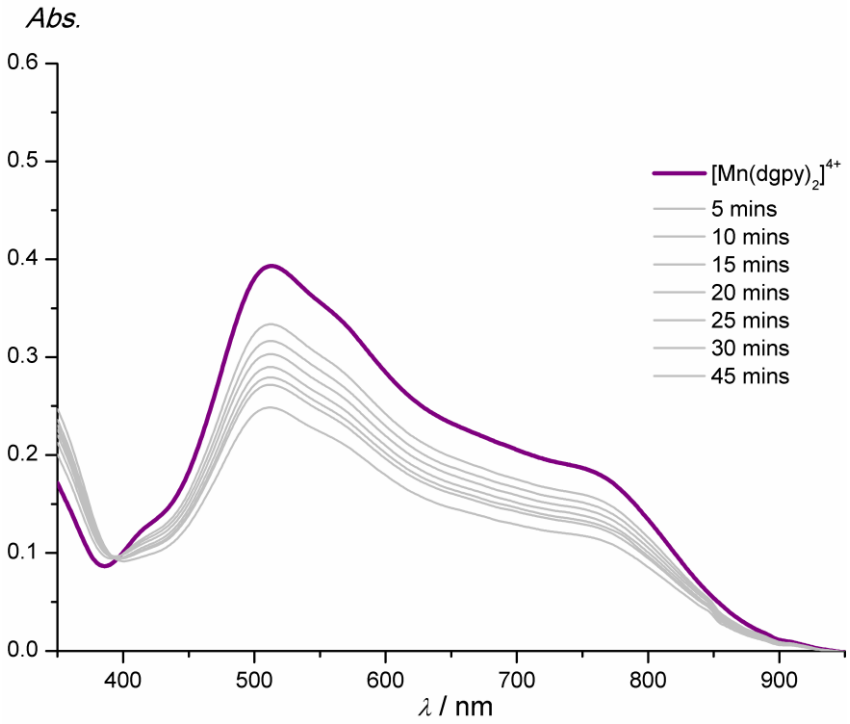

Figure 41. Absorption spectra of $[Mn(dgpy)_2][PF_6]_4$ in the presence of 100 mM $[n\text{-}Bu_4N][PF_6]$ (purple: before irradiation) during irradiation with the 730 nm LED in CH_3CN.

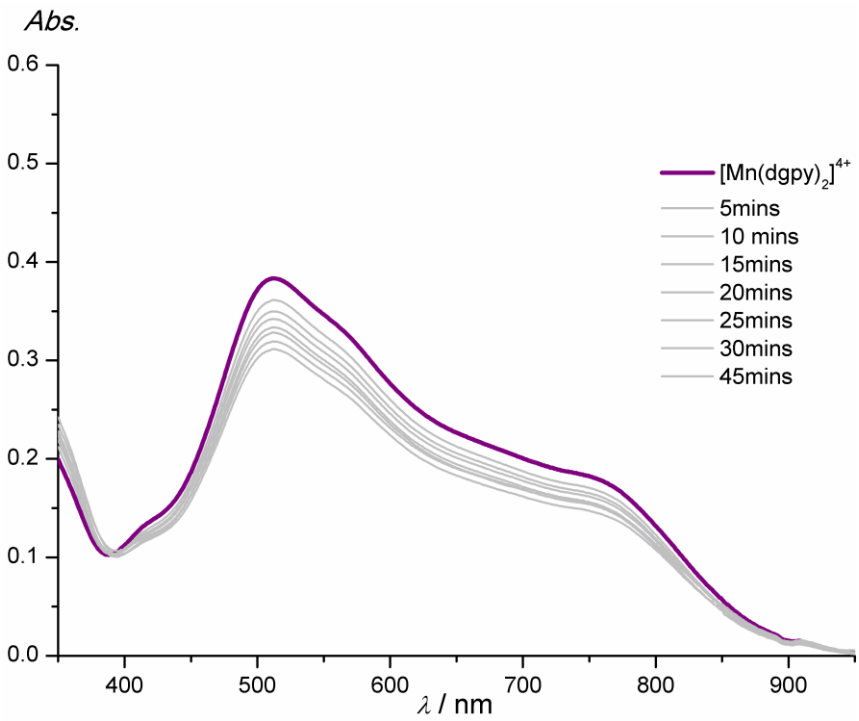

Figure 42. Absorption spectra of $[Mn(dgpy)_2][PF_6]_4$ in the presence of 200 mM $[n\text{-}Bu_4N][PF_6]$ (purple: before irradiation) during irradiation with the 730 nm LED in CH_3CN.

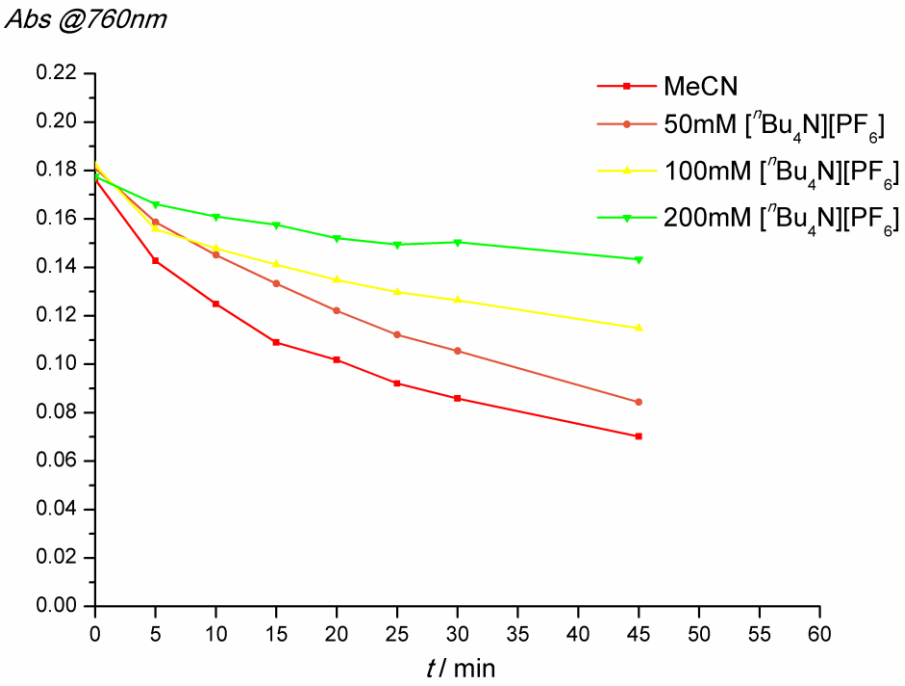

Figure 43. Kinetic traces observed at 760 nm of $[Mn(dgpy)_2][PF_6]_4$ in the presence of 0, 50, 100 and 200 mM $[n\text{-}Bu_4N][PF_6]$ (in red, orange, yellow and green) under irradiation with 730 nm in CH_3CN.

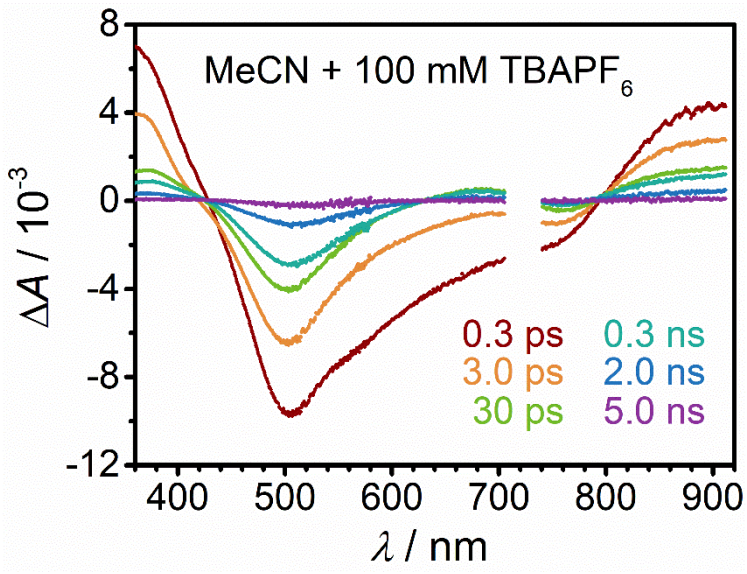

Figure 44. Transient absorption spectra of $[Mn(dgpy)_2][PF_6]_4$ in CH_3CN in the presence of 100 mM $[n\text{-}Bu_4N][PF_6]_4$ after excitation with 730 nm laser pulses of ca. 200 fs duration (800 nJ / pulse).

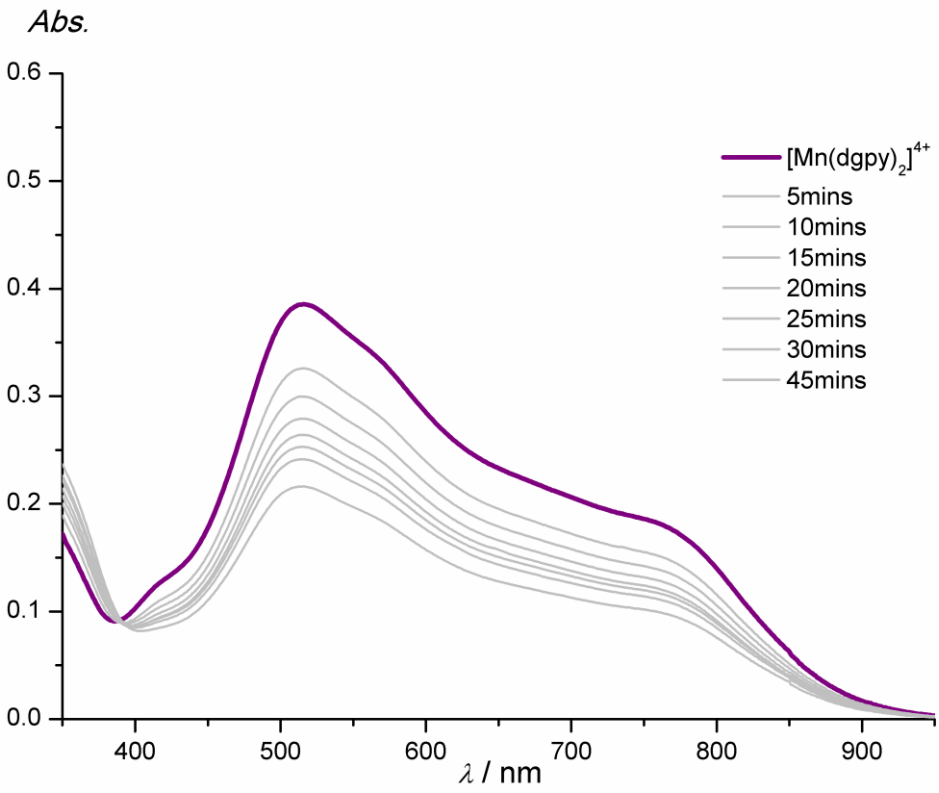

Figure 45. Absorption spectra of $[Mn(dgpy)_2][PF_6]_4$ (purple: before irradiation; orange: after 45 min irradiation) during irradiation with the 730 nm LED in CH_3CN/o-dichlorobenzene 1:1 v/v.

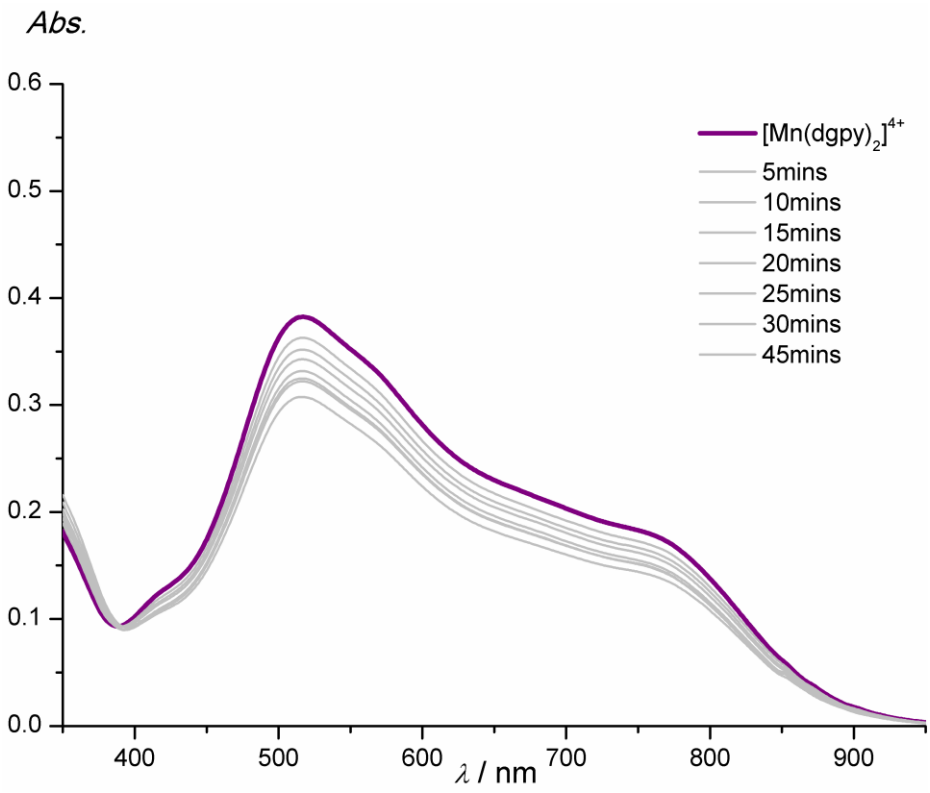

Figure 46. Absorption spectra of $[Mn(dgpy)_2][PF_6]_4$ (purple: before irradiation; orange: after 45 min irradiation) during irradiation with the 730 nm LED in CH_3CN/o-dichlorobenzene 1:2 v/v.

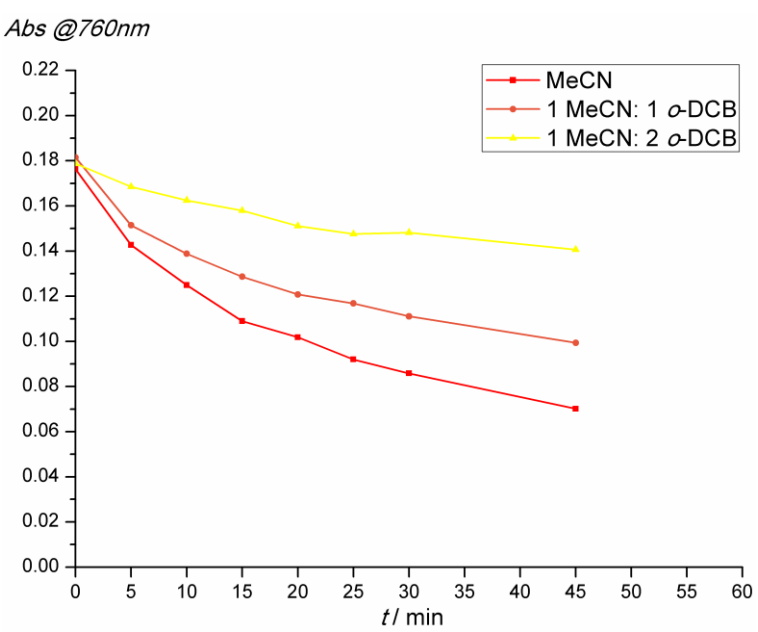

Figure 47. Kinetic traces observed at 760 nm of $[Mn(dgpy)_2][PF_6]_4$ under irradiation with 730 nm in CH_3CN (red), CH_3CN/o-dichlorobenzene 1:1 v/v (orange) and CH_3CN/o-dichlorobenzene 1:2 v/v (yellow).

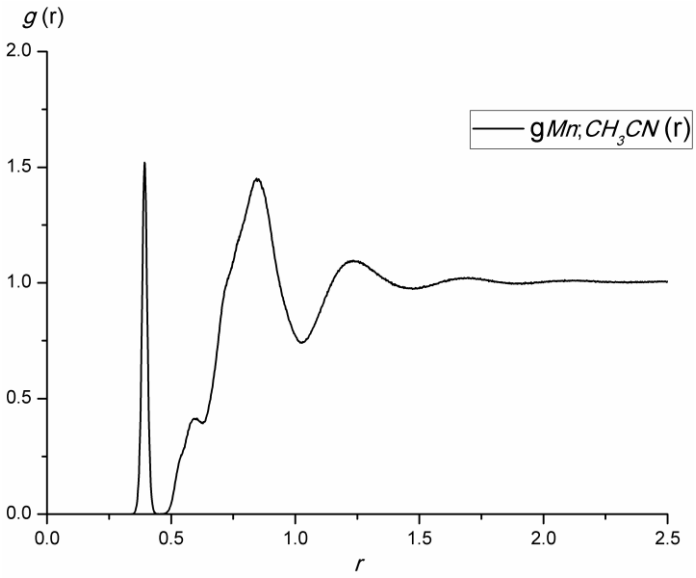

Figure 48. Radial distribution $g(r)$ of CH_3CN molecules (center of mass) from the Mn center in a molecular dynamics simulation of $[Mn(dgpy)_2][PF_6]_4$ in CH_3CN with maxima at 0.39, 0.60, 0.85, 1.23 and 1.68 nm (sampling time 1 µs). The number of CH_3CN molecules $n(r)$ up to a distance r is given by

$n(r) = \rho \cdot (4\pi) \cdot \int_0^r dr'(r')^2 g(r')$, with the particle density ρ = 1761/160.1 nm^{-3} = 11 nm^{-3},

giving n(4.25 Å) = 0.9; n(6.28 Å) = 2.7 and n(10.20 Å) = 41.6.

3. Cartesian coordinates of DFT-UKS calculated geometries

$[Mn(dgpy)_2]^{4+}$ (quartet ground state)[2]

25	-0.089767000	-0.595322000	-0.093908000
6	0.793990000	-3.122292000	-1.221706000
6	0.677685000	-4.446338000	-1.625940000
6	-0.518903000	-5.105611000	-1.439479000
6	-1.594411000	-4.445407000	-0.878267000
6	-1.460981000	-3.110711000	-0.531811000
7	-0.272687000	-2.471064000	-0.692262000
1	1.502521000	-4.954604000	-2.089122000
1	-2.515595000	-4.971210000	-0.705877000
6	1.239397000	0.982954000	-2.225994000
6	2.057382000	0.908998000	-3.493481000
6	3.437059000	0.431928000	-3.114805000
7	3.329282000	-0.838314000	-2.378917000
6	2.198260000	-1.184768000	-1.757050000
7	1.213504000	-0.319725000	-1.532557000
1	4.051803000	0.230115000	-3.989666000
1	1.667344000	1.741093000	-1.569767000
1	2.108866000	1.894343000	-3.951876000
6	-2.537959000	-1.567773000	1.024507000
7	-3.637306000	-1.341569000	1.741998000
6	-3.620945000	-0.591489000	3.013892000
6	-2.384635000	0.260844000	3.164305000
6	-1.176447000	-0.513973000	2.693965000
7	-1.371036000	-0.996148000	1.311176000
1	-3.689944000	-1.327485000	3.818347000
1	-1.009171000	-1.380337000	3.335832000
6	1.267787000	1.748829000	0.927971000
6	1.406647000	3.061014000	1.359018000
6	0.308619000	3.894794000	1.338909000
6	-0.909608000	3.426262000	0.896147000
6	-1.022411000	2.108086000	0.475481000
7	0.062303000	1.286056000	0.498576000
1	2.345817000	3.427995000	1.727743000
1	-1.751541000	4.090636000	0.856237000
6	1.228838000	-2.421228000	1.841602000
6	2.087419000	-2.455703000	3.083661000
6	3.501240000	-2.138296000	2.662998000
7	3.521262000	-0.891017000	1.879615000
6	2.409816000	-0.384842000	1.334461000
7	1.297170000	-1.096560000	1.194898000
1	4.150633000	-1.970296000	3.520513000
1	1.575781000	-3.187096000	1.147429000
1	2.041912000	-3.444926000	3.534833000
6	-2.457685000	0.812463000	-1.034370000
7	-3.614002000	0.853620000	-1.719229000
6	-3.733401000	0.256144000	-3.060321000
6	-2.366364000	0.050541000	-3.659405000
6	-1.542665000	-0.721269000	-2.658364000
7	-1.471832000	-0.011963000	-1.366804000
1	-4.315300000	0.950014000	-3.663194000
1	-2.444200000	-0.513240000	-4.586151000
1	-0.530182000	-0.877641000	-3.012180000
7	2.045533000	-2.494897000	-1.325129000
7	-2.595379000	-2.412778000	-0.068437000
6	-3.896047000	-2.934184000	-0.565309000
1	-4.053966000	-3.941051000	-0.184139000
1	-3.839355000	-2.974111000	-1.651975000
1	-0.616955000	-6.139191000	-1.737436000
1	0.402724000	4.917797000	1.672319000
7	-2.288524000	1.656988000	0.050704000
7	2.414269000	0.931841000	0.891682000
6	3.701828000	1.672791000	0.822053000
6	-3.445028000	2.470747000	0.529068000
1	-3.449415000	3.445955000	0.054052000
1	-3.334393000	2.612557000	1.603762000
6	4.524246000	-1.686215000	-2.440438000
6	4.506386000	-2.649162000	-1.281296000
6	3.212527000	-3.418264000	-1.347430000
1	3.098704000	-4.098566000	-0.507059000
1	4.602518000	-2.116240000	-0.336276000
1	4.554261000	-2.212129000	-3.396627000
1	5.381399000	-1.016212000	-2.397112000

6	-4.940181000	-1.921578000	1.405914000
6	-5.046279000	-2.085369000	-0.088466000
1	-5.976019000	-2.587734000	-0.346499000
1	-5.055094000	-1.110504000	-0.580714000
1	-5.067837000	-2.884522000	1.912298000
1	-5.690521000	-1.238874000	1.804404000
1	-4.532142000	-0.001571000	3.046419000
1	3.959128000	1.167763000	-2.498962000
1	1.602590000	0.218828000	-4.206406000
1	0.215861000	1.278726000	-2.430273000
1	3.203708000	-3.998925000	-2.268156000
1	5.334681000	-3.349723000	-1.357913000
1	-0.284247000	0.094640000	2.724752000
1	-2.263216000	0.540901000	4.209377000
1	-2.484103000	1.177038000	2.596133000
1	0.192726000	-2.642942000	2.065151000
1	1.733564000	-1.725726000	3.813079000
1	3.932376000	-2.945537000	2.067110000
6	4.860451000	0.725325000	0.656617000
6	4.832193000	-0.236149000	1.817065000
1	5.569892000	-1.028856000	1.700957000
1	5.783923000	1.300166000	0.667054000
1	4.809459000	0.192385000	-0.292669000
1	3.852558000	2.235214000	1.741508000
1	3.621005000	2.373648000	-0.004714000
1	5.032172000	0.273757000	2.761356000
6	-4.762384000	1.809632000	0.197036000
6	-4.796618000	1.618961000	-1.299734000
1	-5.565964000	2.471453000	0.512504000
1	-4.893823000	0.866074000	0.729763000
1	-5.685069000	1.070422000	-1.648016000
1	-4.810741000	2.587762000	-1.811251000
1	-4.284897000	-0.685982000	-3.005936000
1	-1.905910000	1.014112000	-3.881004000
1	-1.986093000	-1.705703000	-2.514812000

$[Mn(dgpy)_2]^{4+}$ (^{2}LMCT state)

25	-0.105301000	-0.570224000	-0.114788000
6	0.760718000	-3.103144000	-1.257871000
6	0.635014000	-4.409808000	-1.712963000
6	-0.570809000	-5.059857000	-1.562967000
6	-1.636055000	-4.407720000	-0.980355000
6	-1.483904000	-3.090573000	-0.561708000
7	-0.291391000	-2.455081000	-0.698771000
1	1.456078000	-4.910899000	-2.190735000
1	-2.563895000	-4.930516000	-0.846559000
6	1.267214000	1.004862000	-2.206924000
6	2.103383000	0.960357000	-3.464518000
6	3.467840000	0.442216000	-3.086946000
7	3.329466000	-0.842507000	-2.388553000
6	2.192264000	-1.180707000	-1.770654000
7	1.217958000	-0.304358000	-1.536046000
1	4.084499000	0.251110000	-3.963485000
1	1.684440000	1.749236000	-1.529786000
1	2.182705000	1.960425000	-3.886633000
6	-2.535857000	-1.586688000	1.065549000
7	-3.609121000	-1.463181000	1.852793000
6	-3.606044000	-0.681215000	3.101185000
6	-2.436865000	0.270270000	3.179622000
6	-1.196872000	-0.428103000	2.669262000
7	-1.396362000	-0.940662000	1.300228000
1	-3.584936000	-1.393545000	3.928573000
1	-0.951842000	-1.268704000	3.322064000
6	1.278889000	1.774047000	0.919039000
6	1.428164000	3.096532000	1.326252000
6	0.357902000	3.957529000	1.231596000
6	-0.851795000	3.500587000	0.752783000
6	-0.976257000	2.164565000	0.394103000
7	0.079974000	1.316551000	0.472092000
1	2.360852000	3.450878000	1.722445000
1	-1.673097000	4.183801000	0.645319000
6	1.196025000	-2.409675000	1.824185000
6	2.031540000	-2.474116000	3.082174000
6	3.450161000	-2.141804000	2.697287000
7	3.480462000	-0.878577000	1.948123000
6	2.382064000	-0.373890000	1.368632000

7	1.274167000	-1.079282000	1.192335000
1	4.083741000	-1.997435000	3.571762000
1	1.552848000	-3.169729000	1.129545000
1	1.982930000	-3.474838000	3.507815000
6	-2.430165000	0.852754000	-1.088878000
7	-3.582986000	0.886198000	-1.762132000
6	-3.739145000	0.204037000	-3.053623000
6	-2.386604000	0.028701000	-3.693154000
6	-1.506117000	-0.694215000	-2.702666000
7	-1.451951000	-0.008136000	-1.401145000
1	-4.393259000	0.834249000	-3.653586000
1	-2.471300000	-0.561436000	-4.603516000
1	-0.486824000	-0.793946000	-3.065193000
7	2.022120000	-2.489364000	-1.352568000
7	-2.606854000	-2.419418000	-0.041562000
6	-3.916536000	-2.957925000	-0.504777000
1	-4.021566000	-3.986664000	-0.169424000
1	-3.901623000	-2.941840000	-1.592201000
1	-0.681621000	-6.080085000	-1.901621000
1	0.465733000	4.990670000	1.529492000
7	-2.243152000	1.714011000	-0.026510000
7	2.412022000	0.947363000	0.936991000
6	3.709274000	1.672319000	0.894138000
6	-3.382979000	2.568180000	0.399653000
1	-3.381348000	3.494689000	-0.175091000
1	-3.231742000	2.808247000	1.446781000
6	4.528395000	-1.686258000	-2.420936000
6	4.475871000	-2.684342000	-1.292939000
6	3.172153000	-3.429913000	-1.403779000
1	3.041556000	-4.137268000	-0.589002000
1	4.557901000	-2.184309000	-0.329617000
1	4.594701000	-2.184205000	-3.390759000
1	5.382556000	-1.016966000	-2.326341000
6	-4.882469000	-2.133067000	1.561108000
6	-5.070347000	-2.178176000	0.064675000
1	-5.995167000	-2.691397000	-0.191928000
1	-5.118120000	-1.169671000	-0.341032000
1	-4.885657000	-3.135473000	1.994901000
1	-5.661953000	-1.551571000	2.045339000
1	-4.551496000	-0.144411000	3.146503000
1	4.000047000	1.147202000	-2.444116000
1	1.643175000	0.308630000	-4.209215000
1	0.245660000	1.308945000	-2.418642000
1	3.163097000	-3.972360000	-2.348352000
1	5.296833000	-3.393360000	-1.377455000
1	-0.348477000	0.240708000	2.672200000
1	-2.290235000	0.579742000	4.213249000
1	-2.633406000	1.164769000	2.595413000
1	0.154172000	-2.625719000	2.026007000
1	1.660249000	-1.766514000	3.825196000
1	3.892224000	-2.931668000	2.085326000
6	4.855447000	0.711218000	0.729246000
6	4.806801000	-0.258035000	1.881344000
1	5.522932000	-1.069256000	1.752481000
1	5.789304000	1.269454000	0.743980000
1	4.791758000	0.185687000	-0.221309000
1	3.855801000	2.223952000	1.822054000
1	3.650070000	2.376877000	0.068285000
1	5.025827000	0.238968000	2.829151000
6	-4.687920000	1.850066000	0.179709000
6	-4.800671000	1.556726000	-1.292102000
1	-5.506085000	2.492324000	0.498253000
1	-4.726846000	0.933170000	0.766146000
1	-5.628657000	0.883102000	-1.510849000
1	-4.945387000	2.470295000	-1.872285000
1	-4.240772000	-0.752958000	-2.895360000
1	-1.961176000	0.999879000	-3.951399000
1	-1.885533000	-1.705819000	-2.561262000

$[Mn(dgpy)_2]^{4+}$ (^{6}LMCT state)

25	0.393339000	-0.308526000	0.353453000
6	1.680699000	-3.024355000	0.042295000
6	1.791418000	-4.411546000	0.008249000
6	0.690080000	-5.168392000	0.360387000
6	-0.495059000	-4.554435000	0.719844000
6	-0.556457000	-3.164829000	0.701061000

7	0.522227000	-2.435038000	0.373377000
6	1.605201000	0.627933000	-2.205272000
6	2.525711000	0.308965000	-3.361318000
6	3.923116000	0.174181000	-2.808482000
7	3.930030000	-0.807718000	-1.718243000
6	2.808511000	-1.112978000	-1.045526000
7	1.700685000	-0.386848000	-1.141347000
6	-1.845642000	-1.418398000	1.860130000
7	-2.911490000	-1.333416000	2.666995000
6	-3.129806000	-0.227271000	3.610485000
6	-2.195890000	0.931435000	3.348977000
6	-0.819301000	0.395531000	3.017829000
7	-0.867165000	-0.524613000	1.868530000
6	1.373221000	2.670361000	0.413725000
6	1.345579000	4.072180000	0.154806000
6	0.135283000	4.687683000	-0.067445000
6	-1.015490000	3.933515000	-0.090101000
6	-0.916999000	2.520118000	0.058775000
7	0.251908000	1.932199000	0.332582000
6	2.108022000	-0.975534000	2.735052000
6	2.647240000	-0.358920000	4.009993000
6	3.963464000	0.295644000	3.671249000
7	3.859862000	1.081724000	2.433405000
6	2.765508000	1.016894000	1.646994000
7	1.884980000	0.064180000	1.713944000
6	-2.168100000	0.598782000	-0.881078000
7	-3.351310000	0.346461000	-1.469983000
6	-3.455240000	-0.625470000	-2.566200000
6	-2.095346000	-0.892940000	-3.163023000
6	-1.153374000	-1.231219000	-2.028745000
7	-1.106203000	-0.146353000	-1.032975000
7	2.822250000	-2.237063000	-0.226860000
7	-1.775566000	-2.510826000	1.000771000
6	-3.004532000	-3.235458000	0.572469000
7	-2.083743000	1.796807000	-0.121475000
7	2.587737000	2.119182000	0.754066000
6	3.797104000	2.888081000	0.323269000
6	-3.345489000	2.531492000	0.186601000
6	5.250312000	-1.363639000	-1.410976000
6	5.248930000	-1.927364000	-0.012839000
6	4.109667000	-2.908499000	0.075037000
6	-3.983814000	-2.329587000	2.598495000
6	-4.254994000	-2.605528000	1.135544000
6	5.060596000	2.130479000	0.623166000
6	5.066799000	1.837923000	2.100082000
6	-4.496114000	1.564783000	0.288853000
6	-4.639095000	0.908241000	-1.057521000

{[Mn(dgpy)$_2$] / naphthalene}$^{4+}$ (lowest energy doublet state)

25	-0.316098000	-0.534445000	-0.322094000
6	0.673825000	-3.159204000	-1.160652000
6	0.627909000	-4.529715000	-1.405905000
6	-0.515635000	-5.230574000	-1.089894000
6	-1.604552000	-4.565383000	-0.566231000
6	-1.535607000	-3.188325000	-0.384868000
7	-0.401521000	-2.501426000	-0.666082000
1	1.464076000	-5.042682000	-1.843882000
1	-2.485154000	-5.117609000	-0.295248000
6	0.933490000	0.816599000	-2.683617000
6	1.683414000	0.622269000	-3.983710000
6	3.089330000	0.192473000	-3.645538000
7	3.058248000	-0.950002000	-2.728818000
6	1.955079000	-1.237423000	-2.006028000
7	0.950945000	-0.402824000	-1.865816000
1	3.632542000	-0.131570000	-4.533474000
1	1.383241000	1.641961000	-2.130119000
1	1.710675000	1.550367000	-4.550505000
6	-2.655813000	-1.550336000	1.054465000
7	-3.747713000	-1.387362000	1.824773000
6	-3.779407000	-0.463733000	2.967218000
6	-2.655235000	0.546810000	2.918662000
6	-1.380342000	-0.146258000	2.486774000
7	-1.554371000	-0.847025000	1.206835000
1	-3.721911000	-1.060481000	3.880796000
1	-1.080279000	-0.872663000	3.246841000
6	0.908563000	2.020123000	0.384869000

6	0.970374000	3.369167000	0.718647000
6	-0.177353000	4.129484000	0.652142000
6	-1.362121000	3.548781000	0.257296000
6	-1.386329000	2.189770000	-0.053303000
7	-0.260875000	1.436944000	0.020032000
1	1.890212000	3.817364000	1.045911000
1	-2.243158000	4.155812000	0.172192000
6	1.247908000	-1.999961000	1.778541000
6	2.156813000	-1.833602000	2.977552000
6	3.520457000	-1.438755000	2.462990000
7	3.402389000	-0.307541000	1.536987000
6	2.216075000	0.029247000	0.986379000
7	1.169618000	-0.761232000	0.993470000
1	4.177054000	-1.116038000	3.271774000
1	1.631115000	-2.811836000	1.159360000
1	2.224031000	-2.767003000	3.534284000
6	-2.758844000	0.662455000	-1.417755000
7	-3.915531000	0.661841000	-2.128491000
6	-4.048839000	-0.122351000	-3.354639000
6	-2.689146000	-0.442445000	-3.919295000
6	-1.869406000	-1.063525000	-2.813180000
7	-1.783319000	-0.182122000	-1.640821000
1	-4.648021000	0.473743000	-4.045404000
1	-2.781852000	-1.130181000	-4.757639000
1	-0.856755000	-1.271673000	-3.142238000
7	1.885314000	-2.489350000	-1.397169000
7	-2.694470000	-2.516253000	0.053809000
6	-3.972971000	-3.149498000	-0.360058000
1	-4.041445000	-4.148304000	0.064700000
1	-3.957776000	-3.235787000	-1.445039000
1	-0.559440000	-6.298232000	-1.252984000
1	-0.148306000	5.180228000	0.903967000
7	-2.620244000	1.628083000	-0.420775000
7	2.108178000	1.287465000	0.393927000
6	3.331614000	2.091493000	0.169880000
6	-3.813933000	2.417841000	-0.039953000
1	-3.899277000	3.303334000	-0.670831000
1	-3.678571000	2.742195000	0.986850000
6	4.309306000	-1.704797000	-2.663904000
6	4.344142000	-2.519155000	-1.396307000
6	3.089897000	-3.351298000	-1.357775000
1	3.030475000	-3.944179000	-0.448122000
1	4.407244000	-1.872347000	-0.522653000
1	4.403940000	-2.344779000	-3.545326000
1	5.120453000	-0.976807000	-2.691419000
6	-4.976972000	-2.154445000	1.614699000
6	-5.164174000	-2.369612000	0.131219000
1	-6.064891000	-2.948883000	-0.064629000
1	-5.257052000	-1.413717000	-0.380720000
1	-4.930574000	-3.108421000	2.146638000
1	-5.791323000	-1.572729000	2.039043000
1	-4.748736000	0.033172000	2.957278000
1	3.651160000	1.012419000	-3.190082000
1	1.189648000	-0.134933000	-4.595797000
1	-0.104122000	1.079473000	-2.861665000
1	3.097176000	-4.027086000	-2.213867000
1	5.209766000	-3.178802000	-1.392975000
1	-0.567810000	0.562092000	2.386475000
1	-2.529712000	0.995822000	3.903088000
1	-2.894534000	1.344904000	2.222606000
1	0.240704000	-2.272199000	2.073974000
1	1.764360000	-1.065078000	3.646106000
1	4.004135000	-2.275812000	1.952496000
6	4.526787000	1.191700000	-0.007812000
6	4.665026000	0.373158000	1.251166000
1	5.426772000	-0.400111000	1.142721000
1	5.415051000	1.800739000	-0.163696000
1	4.398146000	0.547723000	-0.876476000
1	3.520797000	2.745727000	1.021668000
1	3.153568000	2.706657000	-0.709008000
1	4.947375000	1.003826000	2.098474000
6	-5.059991000	1.585282000	-0.188007000
6	-5.184997000	1.208853000	-1.640977000
1	-5.923474000	2.167703000	0.126517000
1	-4.999320000	0.699106000	0.442153000
1	-5.943426000	0.439415000	-1.792139000
1	-5.464005000	2.072678000	-2.247091000
1	-4.610445000	-1.036536000	-3.139903000
1	-2.198701000	0.462221000	-4.274641000

1	-2.315782000	-2.015117000	-2.524407000
6	-1.104922000	4.361931000	-3.240686000
6	-2.470587000	4.433566000	-3.007430000
6	-0.618362000	3.647908000	-4.336693000
1	-2.847911000	4.996585000	-2.166264000
1	0.445464000	3.605003000	-4.524838000
6	-3.365829000	3.780851000	-3.856517000
6	-1.497983000	2.979896000	-5.208074000
1	-4.429522000	3.834419000	-3.668222000
6	-2.900712000	3.049485000	-4.964233000
1	-0.413437000	4.859853000	-2.576650000
6	-3.781944000	2.382611000	-5.834786000
1	-4.847321000	2.445745000	-5.658207000
6	-1.031597000	2.237328000	-6.309171000
6	-3.292221000	1.646355000	-6.916377000
1	0.032665000	2.179385000	-6.493508000
1	-3.983376000	1.132964000	-7.569311000
6	-1.926118000	1.574104000	-7.151321000
1	-1.549144000	1.003961000	-7.988272000

$[Mn(dgpy)_2]^{3+}$ (lowest energy triplet state, low-spin)

25	0.386304000	-0.211860000	0.410843000
6	1.684373000	-2.814635000	0.097648000
6	1.792162000	-4.203104000	0.090437000
6	0.713011000	-4.961717000	0.489789000
6	-0.460361000	-4.341405000	0.864501000
6	-0.542071000	-2.953316000	0.812845000
7	0.526424000	-2.204534000	0.445514000
1	2.695427000	-4.687169000	-0.232438000
1	-1.291181000	-4.934089000	1.198964000
6	1.590663000	0.816944000	-2.131136000
6	2.420041000	0.476749000	-3.350537000
6	3.846901000	0.285590000	-2.896456000
7	3.893052000	-0.676463000	-1.791541000
6	2.794395000	-0.946109000	-1.053632000
7	1.704577000	-0.217320000	-1.093916000
1	4.470378000	-0.120538000	-3.693199000
1	1.919383000	1.777755000	-1.733986000
1	2.362722000	1.282077000	-4.081236000
6	-1.889800000	-1.217511000	1.907430000
7	-3.020641000	-1.050369000	2.621672000
6	-3.187718000	0.046459000	3.584725000
6	-2.209693000	1.172250000	3.337252000
6	-0.843464000	0.586181000	3.053527000
7	-0.885270000	-0.371378000	1.939174000
1	-3.057537000	-0.363207000	4.589629000
1	-0.469733000	0.074014000	3.944338000
6	1.307095000	2.553394000	0.621893000
6	1.217387000	3.942246000	0.634795000
6	0.017043000	4.540079000	0.316626000
6	-1.077633000	3.759983000	0.014566000
6	-0.962344000	2.371577000	0.069752000
7	0.222659000	1.780800000	0.362478000
1	2.064836000	4.549582000	0.893148000
1	-1.999341000	4.230130000	-0.272575000
6	1.988006000	-1.066691000	2.797277000
6	2.822550000	-0.589021000	3.965564000
6	4.159311000	-0.150040000	3.417809000
7	3.964728000	0.783555000	2.303305000
6	2.778616000	0.876279000	1.662340000
7	1.821816000	-0.010570000	1.790796000
1	4.749100000	0.374658000	4.169939000
1	2.475753000	-1.933434000	2.349967000
1	2.959613000	-1.393234000	4.686782000
6	-2.133548000	0.442509000	-0.918455000
7	-3.276487000	0.124117000	-1.565615000
6	-3.294779000	-0.907912000	-2.606118000
6	-1.903011000	-1.108224000	-3.153529000
6	-0.985192000	-1.367596000	-1.979849000
7	-1.043016000	-0.282283000	-0.990643000
1	-3.984376000	-0.563454000	-3.376871000
1	-1.885268000	-1.954704000	-3.838421000
1	0.047557000	-1.464565000	-2.299977000
7	2.828880000	-2.065043000	-0.221654000
7	-1.781287000	-2.350445000	1.104574000
6	-2.967357000	-3.186652000	0.789606000

1	-2.951849000	-4.091846000	1.392703000
1	-2.898302000	-3.469106000	-0.259195000
1	0.785426000	-6.040108000	0.507964000
1	-0.064986000	5.617820000	0.299611000
7	-2.123256000	1.612128000	-0.154492000
7	2.572348000	1.980260000	0.835309000
6	3.716559000	2.851271000	0.478581000
6	-3.393407000	2.353940000	0.021551000
1	-3.533673000	3.060533000	-0.798686000
1	-3.316487000	2.916589000	0.947206000
6	5.213904000	-1.253533000	-1.543521000
6	5.270082000	-1.806928000	-0.142182000
6	4.114940000	-2.760741000	0.014593000
1	4.075262000	-3.180313000	1.016998000
1	5.209576000	-1.006386000	0.594232000
1	5.425556000	-2.031891000	-2.281662000
1	5.941712000	-0.454193000	-1.684933000
6	-4.153324000	-1.972085000	2.524391000
6	-4.251338000	-2.463674000	1.099575000
1	-5.081142000	-3.158724000	0.984110000
1	-4.410467000	-1.625656000	0.423694000
1	-4.032320000	-2.806478000	3.220769000
1	-5.041313000	-1.417287000	2.816776000
1	-4.215037000	0.398428000	3.502505000
1	4.287487000	1.233569000	-2.575918000
1	2.047164000	-0.436210000	-3.819037000
1	0.539441000	0.916795000	-2.384202000
1	4.241625000	-3.576484000	-0.698096000
1	6.202744000	-2.344898000	0.016266000
1	-0.130532000	1.364273000	2.813859000
1	-2.171737000	1.819014000	4.212996000
1	-2.533877000	1.777027000	2.494784000
1	1.000660000	-1.384413000	3.113647000
1	2.326502000	0.242289000	4.470392000
1	4.741390000	-1.008583000	3.072339000
6	5.011807000	2.085239000	0.543118000
6	5.154905000	1.555192000	1.947239000
1	6.008412000	0.881973000	2.033495000
1	5.835197000	2.755620000	0.304264000
1	5.016178000	1.270504000	-0.179039000
1	3.784107000	3.692825000	1.168609000
1	3.525994000	3.237017000	-0.520153000
1	5.298722000	2.371035000	2.660921000
6	-4.562097000	1.404925000	0.051512000
6	-4.592621000	0.691535000	-1.274270000
1	-5.480364000	1.970321000	0.198259000
1	-4.463287000	0.697590000	0.874845000
1	-5.303420000	-0.135738000	-1.267677000
1	-4.882342000	1.374227000	-2.077468000
1	-3.692545000	-1.837702000	-2.190380000
1	-1.580883000	-0.220181000	-3.701296000
1	-1.266219000	-2.312507000	-1.515329000

$[Mn(dgpy)_2]^{3+}$ (lowest energy quintet state, high-spin)[2]

25	0.383227000	-0.222053000	0.339033000
6	1.724579000	-2.991375000	0.097939000
6	1.873696000	-4.374682000	0.224909000
6	0.796139000	-5.116912000	0.670579000
6	-0.409862000	-4.495693000	0.946821000
6	-0.510094000	-3.128391000	0.736524000
7	0.543658000	-2.407038000	0.333992000
1	2.798513000	-4.867349000	-0.015745000
1	-1.233293000	-5.060100000	1.352416000
6	1.679330000	0.693798000	-2.188187000
6	2.457343000	0.276959000	-3.416565000
6	3.884487000	0.034653000	-2.986933000
7	3.924212000	-0.815406000	-1.788587000
6	2.810848000	-1.094134000	-1.075858000
7	1.718409000	-0.359299000	-1.162320000
1	4.455059000	-0.486069000	-3.757353000
1	2.105559000	1.616094000	-1.790836000
1	2.420902000	1.058636000	-4.173100000
6	-1.877815000	-1.390769000	1.790245000
7	-2.999865000	-1.293249000	2.519317000
6	-3.211224000	-0.250558000	3.532549000
6	-2.241560000	0.903500000	3.386637000

6	-0.866122000	0.365982000	3.041418000
7	-0.894558000	-0.511979000	1.860356000
1	-3.097170000	-0.719661000	4.512864000
1	-0.472149000	-0.201718000	3.888082000
6	1.370787000	2.705092000	0.478209000
6	1.339243000	4.095341000	0.359929000
6	0.135363000	4.705123000	0.068133000
6	-1.008365000	3.947926000	-0.097575000
6	-0.914493000	2.565776000	0.041769000
7	0.256928000	1.973398000	0.320305000
1	2.214748000	4.697821000	0.514071000
1	-1.934427000	4.429422000	-0.353077000
6	2.049188000	-0.969168000	2.722886000
6	2.613582000	-0.352879000	3.987609000
6	3.967048000	0.220212000	3.632845000
7	3.898092000	0.955105000	2.358476000
6	2.767108000	0.999987000	1.615524000
7	1.840746000	0.071703000	1.706039000
1	4.319411000	0.927301000	4.386226000
1	2.751791000	-1.717483000	2.347360000
1	2.714539000	-1.102229000	4.770238000
6	-2.172903000	0.632515000	-0.853323000
7	-3.371625000	0.313771000	-1.394068000
6	-3.475456000	-0.693400000	-2.452997000
6	-2.141321000	-0.913650000	-3.119840000
6	-1.115930000	-1.177278000	-2.040598000
7	-1.093382000	-0.102443000	-1.037459000
1	-4.220614000	-0.339157000	-3.163774000
1	-2.201961000	-1.762680000	-3.798309000
1	-0.116756000	-1.261430000	-2.459742000
7	2.847388000	-2.206341000	-0.233006000
7	-1.758579000	-2.479667000	0.935079000
6	-2.944344000	-3.210203000	0.419470000
1	-2.898622000	-4.255656000	0.723285000
1	-2.902708000	-3.188814000	-0.669614000
1	0.900411000	-6.183294000	0.815263000
1	0.088962000	5.780043000	-0.036678000
7	-2.095807000	1.791206000	-0.083440000
7	2.610653000	2.071077000	0.727782000
6	3.796891000	2.889213000	0.383998000
6	-3.343648000	2.539038000	0.189732000
1	-3.557861000	3.237380000	-0.620579000
1	-3.178107000	3.110158000	1.095077000
6	5.258319000	-1.326489000	-1.471042000
6	5.272082000	-1.855084000	-0.059906000
6	4.148414000	-2.851514000	0.055266000
1	4.086259000	-3.266580000	1.058236000
1	5.145415000	-1.044435000	0.659696000
1	5.539638000	-2.105585000	-2.183856000
1	5.953153000	-0.495243000	-1.597665000
6	-4.045619000	-2.312409000	2.408222000
6	-4.232422000	-2.611211000	0.936020000
1	-5.045028000	-3.314215000	0.764770000
1	-4.472091000	-1.685644000	0.411339000
1	-3.759724000	-3.211059000	2.959307000
1	-4.946555000	-1.901307000	2.853929000
1	-4.242760000	0.086193000	3.448219000
1	4.395123000	0.977201000	-2.773231000
1	2.027074000	-0.629736000	-3.845166000
1	0.638569000	0.898195000	-2.419360000
1	4.326926000	-3.668606000	-0.644818000
1	6.216875000	-2.350330000	0.154984000
1	-0.176970000	1.178417000	2.844651000
1	-2.202189000	1.455504000	4.328261000
1	-2.574298000	1.606781000	2.621322000
1	1.105833000	-1.471061000	2.900992000
1	1.945199000	0.428956000	4.350432000
1	4.715543000	-0.570229000	3.544079000
6	5.067195000	2.098995000	0.571403000
6	5.121303000	1.681964000	2.020341000
1	5.955008000	1.006398000	2.216551000
1	5.918429000	2.728884000	0.321021000
1	5.094229000	1.226979000	-0.083271000
1	3.849837000	3.769376000	1.024983000
1	3.672995000	3.221027000	-0.644786000
1	5.235737000	2.552976000	2.670542000
6	-4.498685000	1.580651000	0.343478000
6	-4.661887000	0.882095000	-0.983326000
1	-5.404001000	2.121711000	0.619618000

1	-4.259109000	0.865855000	1.128374000
1	-5.372790000	0.054990000	-0.932071000
1	-5.021803000	1.582612000	-1.741898000
1	-3.863071000	-1.626829000	-2.030602000
1	-1.861609000	-0.032632000	-3.702500000
1	-1.326014000	-2.130937000	-1.557647000

4. References

1. Van Duyne, R. P. & Reilly, C. N. Low-temperature electrochemistry. I. Characteristics of electrode reactions in the absence of coupled chemical kinetics. *Anal. Chem.* **44**, 142–152 (1972).

2. East, N. R., Förster, C., Carrella, L. M., Rentschler, E. & Heinze, K. The full d^3–d^5 Redox Series of Mononuclear Manganese Complexes: Geometries and Electronic Structures of $[Mn(dgpy)_2]^{n+}$. *Inorg. Chem.* **61**, 14616−14625 (2022).

3. Fulmer, G. R., Miller, A. J. M., Sherden, N. H., Gottlieb, H. E., Nudelman, A., Stoltz, B. M., Bercaw, J. E. & Goldberg, K. I. NMR Chemical Shifts of Trace Impurities: Common Laboratory Solvents, Organics, and Gases in Deuterated Solvents Relevant to the Organometallic Chemist. *Organometallics* **29**, 2176–2179 (2010).

4. Snellenburg, J. J., Laptenok, S., Seger, R., Mullen, K. M. & van Stokkum, I. H. M. Glotaran: A Java-Based Graphical User Interface for the R Package TIMP. *J. Stat. Softw.* **49**, 1–22 (2012).

5. https://www.prizmatix.com/LEDUHP/LED-UHP-TLA.aspx (accessed Feb. 21st 2023).

6. Neese, F. Software update: The ORCA program system, version 4.0. *WIREs Comput. Mol. Sci.* **8**, e1327 (2018).

7. Becke, A. D. Density-functional thermochemistry. III. The role of exact exchange. *J. Chem. Phys.* **98**, 5648–5652 (1993).

8. Miehlich, B., Savin, A., Stoll, H. & Preuss, H. Results obtained with the correlation energy density functionals of Becke and Lee, Yang and Parr. *Chem. Phys. Lett.* **157**, 200–206 (1989).

9. Lee, C., Yang, W. & Parr, R. G. Development of the Colle-Salvetti correlation-energy formula into a functional of the electron density. *Phys. Rev. B* **37**, 785–789 (1988).

10. Neese, F., Wennmohs, F., Hansen, A. & Becker, U. Efficient, approximate and parallel Hartree–Fock and hybrid DFT calculations. A 'chain-of-spheres' algorithm for the Hartree–Fock exchange. *Chem. Phys.* **356**, 98–109 (2009).

11. Izsák, R. & Neese, F. An overlap fitted chain of spheres exchange method. *J. Chem. Phys.* **135**, 144105 (2011).

12. Pantazis, D. A., Chen, X.-Y., Landis, C. R. & Neese, F. All-Electron Scalar Relativistic Basis Sets for Third-Row Transition Metal Atoms. *J. Chem. Theory Comput.* **4**, 908–919 (2008).

13. Miertus, S., Scrocco, E. & Tomasi, J. Electrostatic interaction of a solute with a continuum: A direct utilization of ab initio molecular potentials for the prevision of solvent effects. *Chem. Phys.* **55**, 117–129 (1981).

14. Barone, V. & Cossi, M. Quantum Calculation of Molecular Energies and Energy Gradients in Solution by a Conductor Solvent Model. *J. Phys. Chem. A* **102**, 1995–2001 (1998).

15. Weigend, F. Accurate Coulomb-fitting basis sets for H to Rn. *Phys. Chem. Chem. Phys.* **8**, 1057–1065 (2006).

16. Weigend, F. & Ahlrichs, R. Balanced basis sets of split valence, triple zeta valence and quadruple zeta valence quality for H to Rn: Design and assessment of accuracy. *Phys. Chem. Chem. Phys.* **7**, 3297–3305 (2005).

17. Grimme, S., Antony, J., Ehrlich, S. & Krieg, H. A consistent and accurate ab initio parametrization of density functional dispersion correction (DFT-D) for the 94 elements H-Pu. *J. Chem. Phys.* **132**, 154104 (2010).

18. Grimme, S., Ehrlich, S. & Goerigk, L. Effect of the damping function in dispersion corrected density functional theory. *J. Comput. Chem.* **32**, 1456–1465 (2011).

19. Plasser, F. TheoDORE; at http://theodore-qc.sourceforge.net (accessed Feb. 21st 2023).

20. Plasser & F. TheoDORE: A toolbox for a detailed and automated analysis of electronic excited state computations. *J. Chem. Phys.* **152**, 84108 (2020).

21. Hess, B., Kutzner, C., van der Spoel, D. & Lindahl, E. GROMACS 4: Algorithms for Highly Efficient, Load-Balanced, and Scalable Molecular Simulation. *J. Chem. Theory Comput.* **4**, 435–447 (2008).

22. Jorgensen, W. L., Maxwell, D. S. & Tirado-Rives, J. Development and Testing of the OPLS All-Atom Force Field on Conformational Energetics and Properties of Organic Liquids. *J. Am. Chem. Soc.* **118**, 11225–11236 (1996).

23. Shao, Y. et al., Advances in molecular quantum chemistry contained in the Q-Chem 4 program package. *Mol. Phys.* **113**, 184-215 (2015).

24. Darden, T., York, D. & Pedersen, L. Particle mesh Ewald: An N·log(N) method for Ewald sums in large systems. *J. Chem. Phys.* **98**, 10089 (1993).

25. Allen, M. & Tildesley, D. Computer Simulations of Liquids, 2nd edition Oxford Academic (2017).

26. Hess, B., Bekker, H., Berendsen, H. J., Fraaije, J. G. LINCS: A Linear Constraint Solver for Molecular Simulations. *J. Comput. Phys.* **18**, 1463–1472 (1997).

27. Bussi, G., Donadio, D. & Parrinello, M. Canonical sampling through velocity rescaling. *J. Chem. Phys.* **126**, 014101 (2007).

28. Berendsen, H. J. C., Postma, J. P. M., DiNola, A. & Haak, J. R. Molecular dynamics with coupling to an external bath. *J. Chem. Phys.* **81**, 3684 (1984).